POLITECNICO DI TORINO
Repository ISTITUZIONALE

Extreme Event Quantification in Dynamical Systems with Random Components

Original
Extreme Event Quantification in Dynamical Systems with Random Components / Dematteis, Giovanni; Grafke, Tobias; Vanden-Eijnden, Eric. - In: SIAM/ASA JOURNAL ON UNCERTAINTY QUANTIFICATION. - ISSN 2166-2525. - 7:3(2019), pp. 1029-1059. [10.1137/18M1211003]

Availability:
This version is available at: 11583/2751232 since: 2019-09-10T17:56:35Z

Publisher:
Society for Industrial and Applied Mathematics

Published
DOI:10.1137/18M1211003

Terms of use:

This article is made available under terms and conditions as specified in the corresponding bibliographic description in the repository

Publisher copyright

(Article begins on next page)

12 October 2024

SIAM/ASA J. UNCERTAINTY QUANTIFICATION
Vol. 7, No. 3, pp. 1029–1059
© 2019 Society for Industrial and Applied Mathematics
and American Statistical Association

Extreme Event Quantification in Dynamical Systems with Random Components*

Giovanni Dematteis†, Tobias Grafke‡, and Eric Vanden-Eijnden§

Abstract. A central problem in uncertainty quantification is how to characterize the impact that our incomplete knowledge about models has on the predictions we make from them. This question naturally lends itself to a probabilistic formulation, by making the unknown model parameters random with given statistics. Here this approach is used in concert with tools from large deviation theory (LDT) and optimal control to estimate the probability that some observables in a dynamical system go above a large threshold after some time, given the prior statistical information about the system's parameters and/or its initial conditions. Specifically, it is established under which conditions such extreme events occur in a predictable way, as the minimizer of the LDT action functional. It is also shown how this minimization can be numerically performed in an efficient way using tools from optimal control. These findings are illustrated on the examples of a rod with random elasticity pulled by a time-dependent force, and the nonlinear Schrödinger equation with random initial conditions.

Key words. large deviation theory, extreme events, optimal control, nonlinear Schrödinger equation, solitons

AMS subject classifications. 60F10, 65K10, 49J20, 76B25

DOI. 10.1137/18M1211003

1. Introduction.

The governing equations we use to model complex phenomena are often approximate. For example, we may not know exactly the initial and/or boundary conditions necessary to integrate these equations. Other parameters entering these equations can also be uncertain, either because we are not sure of the model itself or because these parameters may vary from situation to situation in a way that is difficult to predict in detail. The question then becomes whether we can quantify how our imperfect knowledge of the system's parameters impact its behavior. This question lends itself naturally to a probabilistic formulation. Consider, for example, the case of a dynamical system whose state at time t can be specified by some $u(t)$ which can be a vector or a field and satisfies

$$\partial_t u = b(u, \vartheta), \qquad u(t=0) = u_0(\vartheta). \tag{1.1}$$

Here $b(u, \vartheta)$ is a given vector field and ϑ denotes the set of parameters we are uncertain of. Assuming that these parameters take value in some set Ω, which can again be finite or infinite dimensional, it is then natural to equip Ω with a probability measure μ to quantify our

*Received by the editors September 4, 2018; accepted for publication (in revised form) May 20, 2019; published electronically August 13, 2019.
https://doi.org/10.1137/18M1211003
Funding: The work of the first author was supported by the joint Math PhD program of Politecnico and Universit di Torino and partially supported by MIUR grant Dipartimenti di Eccellenza 2018-2022. The work of the third author was partially supported by the National Science Foundation Materials Research Science and Engineering Center Program Award DMR-1420073 and DMS-1522767.
†Dipartimento di Scienze Matematiche, Politecnico di Torino, Torino (giovanni.dematteis@polito.it).
‡Mathematics Institute, University of Warwick, Coventry (T.Grafke@warwick.ac.uk).
§NYU, Courant Institute of Mathematical Sciences, New York, NY 10012 (eve2@cims.nyu.edu).

Copyright © by SIAM and ASA. Unauthorized reproduction of this article is prohibited.

Downloaded 09/25/19 to 130.192.92.55. Redistribution subject to SIAM license or copyright; see http://www.siam.org/journals/ojsa.php

Downloaded 09/25/19 to 130.192.92.55. Redistribution subject to SIAM license or copyright; see http://www.siam.org/journals/ojsa.php

uncertainty. This makes ϑ random, and therefore the solution to (1.1) becomes a stochastic process. Denoting it by $u(\cdot, \vartheta)$, we can ask questions about the statistics of this process. For example, if $f(u)$ is a scalar valued observable, we can define

$$P_T(z) \equiv \mathbb{P}\left(f(u(T,\vartheta)) \geq z\right), \qquad z \in \mathbb{R}, \tag{1.2}$$

where $\mathbb{P}$ denotes the probability over μ and $T > 0$ is some observation time. The probability (1.2) is useful, e.g., in the context of a certification problem where, given $z \in \mathbb{R}$ and $\epsilon > 0$ (typically z large and ϵ small), we wish to verify that $P_T(z) \leq \epsilon$. Other quantities of interest include

$$\mathbb{P}\left(\int_0^T f(u(t,\vartheta))dt \geq z\right), \qquad \mathbb{P}\left(\sup_{0\leq t\leq T} f(u(t,\vartheta)) \geq z\right), \qquad \text{etc.} \tag{1.3}$$

The numerical estimation of (1.2) or (1.3) can be performed by Monte Carlo sampling methods: generate N independent realizations of ϑ, for each evaluate $f(u(T,\vartheta))$ via integration of (1.1), and compute the fraction of these realizations for which $f(u(T,\vartheta)) \geq z$. As $N \to \infty$, this fraction will converge to $P_T(z)$. This direct approach is not effective when $P_T(z)$ is small, however, since the relative error of the estimator just described is $\sqrt{(1-P_T(z))/(NP_T(z))} \sim 1/\sqrt{NP_T(z)}$. This means that in order to get an estimate accurate to order $\delta \ll 1$, we need to use $N = O\left(\delta^{-2}P_T^{-1}(z)\right)$ samples, which can become prohibitively expensive as $P_T(z)$ gets smaller. This is problematic since it excludes from consideration events that are rare but may nonetheless have dramatic consequences. Similar issues arise if we replace (1.1) by some time independent equation like

$$0 = b(u,\vartheta), \tag{1.4}$$

where $b(\cdot,\vartheta)$ is some function of u and possibly its derivatives and (1.4) is supplemented with boundary conditions that may also depend on the random parameter ϑ. The solution to (1.4) defines a complicated map $u(\vartheta)$, and given a scalar valued observable $f(u)$, the estimation of

$$\mathbb{P}\left(f(u(\vartheta)) \geq z\right), \qquad z \in \mathbb{R}, \tag{1.5}$$

will again be challenging when this probability is small, i.e., when the event $f(u(\vartheta)) \geq z$ is rare.

In these situations alternative methods such as those proposed, e.g., in [20, 26, 9, 19, 39, 42, 17, 36], must be used to estimate (1.2), (1.3), or (1.5). The approach we introduce in this paper builds on earlier results found in [13] and uses large deviation theory (LDT) [14, 43] as a tool: we show that, if in (1.2) $P_T(z) \to 0$ as $z \to \infty$, then under some additional assumptions we have

$$P_T(z) \asymp \exp\left(-\min_{\theta\in\Omega(z)} I(\theta)\right), \qquad \text{where} \qquad \Omega(z) = \{\theta : f(u(T,\theta)) \geq z\} \subseteq \Omega. \tag{1.6}$$

Here $\asymp$ indicates that the ratio of logarithms of both sides tends to 1 as $z \to \infty$ and we defined

$$I(\theta) = \max_{\eta}\left(\langle \eta, \theta\rangle - S(\eta)\right), \tag{1.7}$$

Copyright © by SIAM and ASA. Unauthorized reproduction of this article is prohibited.

Downloaded 09/25/19 to 130.192.92.55. Redistribution subject to SIAM license or copyright; see http://www.siam.org/journals/ojsa.php

where $\langle \cdot, \cdot \rangle$ is a suitable inner product on Ω and $S(\eta)$ is the cumulant generating function of ϑ:

$$S(\eta) = \log \mathbb{E} e^{\langle \eta, \vartheta \rangle} = \log \int_\Omega e^{\langle \eta, \theta \rangle} d\mu(\theta) \,. \tag{1.8}$$

We will also show that the minimizer of $I(\theta)$ in $\Omega(z)$, i.e.,

$$\theta^\star(z) = \operatorname*{argmin}_{\theta \in \Omega(z)} I(\theta) \,, \tag{1.9}$$

is the point of maximum likelihood in $\Omega(z)$. The most likely way the event $\{f(u(T, \vartheta)) \geq z\}$ occurs is when $\vartheta = \theta^\star(z)$, which we will also refer to as the *instanton* realization, since it is a critical point of the action $I(\theta)$. Similar estimates hold for (1.3) and (1.5) upon straightforward redefinition of the set $\Omega(z)$ upon which the optimization is performed.

Establishing the large deviation principle (LDP) in (1.6) is one of the objectives of this paper. As we will see in section 2, this can be done by proving that $\theta^\star(z)$ is a dominating point in $\Omega(z)$, building on results derived, e.g., in [5, 31, 7, 24] that provide us with a framework to justify the saddle-point approximations often used in physics [25, 18]. Equation (1.6) is a somewhat unusual LDP however because there is no small (or large) parameter associated to the random variable ϑ: rather we play with the variable z being large. More precisely, instead of scaling ϑ so that events with a finite z become rare, we keep ϑ as is and look at rare events that occur in the tail of the distribution when $z \gg 1$. As a result, the standard approach developed in [5, 31, 24] must be adapted. In particular, we do not know a priori what is the speed of the LDP. The formulation we adopt can be viewed as a way to estimate this speed by estimating how the minimum in (1.6) behaves as z increases toward infinity.

When (1.6) holds, we can reduce the evaluation of $P_T(z)$ to the minimization problem in (1.9), and a second objective here is to design numerical tools to perform this minimization. As we will see in section 3, this can be done by adapting techniques used in optimal control [41, 6].

We will also illustrate these tools on two examples in section 4: The first one is a model for an elastic rod with a random elasticity coefficient. The rod gets pulled from one end with a given forcing protocol, and the response depends nonlinearly on the elasticity coefficient. The LDP can be used here to infer the probability of atypically large extensions of the rod. The second application deals with the nonlinear Schrödinger equation (NLSE) in nonlinear fiber optics, in the context of what is known as integrable turbulence. Specifically, we study the problem of the onset of rogue waves out of a bath of random waves taken as initial condition for NLSE.

2. Large deviation principle.

Here we establish (1.6), using background material that can be found, e.g., in [5, 31, 24]. For simplicity, we will restrict ourselves to situations where ϑ is finite dimensional, i.e., we assume that $\vartheta \in \Omega \subseteq \mathbb{R}^M$ with $M \in \mathbb{N}$. In this case we can also assume that the inner product $\langle \cdot, \cdot \rangle$ appearing in (1.7) and (1.8) is the standard Euclidean inner product on $\mathbb{R}^M$. Under appropriate assumptions, the results below will hold also in the infinite-dimensional set-up, when ϑ is a random field, but the arguments to establish them will require generalization (see, e.g., [15, 29] for results in infinite dimension). To treat the

Copyright © by SIAM and ASA. Unauthorized reproduction of this article is prohibited.

problems in (1.2), (1.3), and (1.5) on the same footing we also define the map $F : \Omega \to \mathbb{R}$ via

$$
\begin{aligned}
&F(\theta) = f(u(T,\theta)) && \text{for (1.2)},\\
&F(\theta) = \int_0^T f(u(t,\theta))\,dt, \quad \text{or} \quad F(\theta) = \sup_{0\le t\le T} f(u(t,\theta)), && \text{for (1.3)},\\
&F(\theta) = f(u(\theta)) && \text{for (1.5)}
\end{aligned}
\tag{2.1}
$$

so that we can recast these probabilities into

$$
P(z) = \mathbb{P}(F(\vartheta) \ge z) = \mu(\Omega(z)), \qquad \text{where} \qquad \Omega(z) = \{\theta \,:\, F(\theta) \ge z\}\,. \tag{2.2}
$$

To proceed, we start by making two assumptions.

Assumption 1. There exists a finite z_0 such that the restriction of the map F to the preimage of the interval $(z_0,\infty) \subset \mathbb{R}$, i.e., to the set $F^{-1}\big((z_0,\infty)\big) \subset \Omega$, is differentiable with $|\nabla(F)| > K$ for a suitable $K > 0$.

Assumption 2. The measure μ is such that (this is (1.8))

$$
S(\eta) = \log \mathbb{E} e^{\langle \eta,\vartheta\rangle} = \log \int_\Omega e^{\langle \eta,\theta\rangle} d\mu(\theta) \tag{2.3}
$$

exists for all $\eta \in \mathbb{R}^M$ and defines a differentiable function $S : \mathbb{R}^M \to \mathbb{R}$.

Ultimately, Assumption 1 is about the specifics of the governing equation in (1.1) or (1.4) and the observable f: since the field u is typically a complicated function of ϑ, establishing the conditions under which this assumption holds will have to be done on a case-by-case basis. Note that it guarantees that the set $\Omega(z)$ is simply connected with a boundary that is C^1 for all $z \in \mathbb{R}$, with inward pointing unit normal at $\theta(z) \in \partial\Omega(z)$ given by $\hat{n}(z) = \nabla F(\theta(z))/|\nabla F(\theta(z))|$. We could relax the constraint $|\nabla F(\theta)| > 0$ and allow, e.g., for the sets $\Omega(z)$ to have several connected components (the number of which could depend on z), but this requires modifying the argument below. Assumption 2 allows us to introduce the tilted measure

$$
d\mu_\eta(\theta) = \frac{e^{\langle \eta,\theta\rangle} d\mu(\theta)}{\int_\Omega e^{\langle \eta,\theta\rangle} d\mu(\theta)} = e^{\langle \eta,\theta\rangle - S(\eta)} d\mu(\theta)\,. \tag{2.4}
$$

It is easy to see that the mean of μ_η is shifted compared to that of μ. A simple calculation shows that

$$
\int_\Omega \theta\, d\mu_\eta(\theta) = \nabla S(\eta)\,, \tag{2.5}
$$

and this will allow us to pick η such that the mean of μ_η is precisely at the point minimizing $I(\theta)$ in $\Omega(z)$. Note that

$$
\Omega(z+\delta) \subseteq \Omega(z) \qquad \forall z \in \mathbb{R}, \delta \ge 0\,, \tag{2.6}
$$

and to establish (1.6) we will find conditions such that (i) $\mu(\Omega(z))$ decreases fast with z and (ii) this probability is dominated by a small region around a single point on $\partial\Omega(z)$. This will

Copyright © by SIAM and ASA. Unauthorized reproduction of this article is prohibited.

Downloaded 09/25/19 to 130.192.92.55. Redistribution subject to SIAM license or copyright; see http://www.siam.org/journals/ojsa.php

Downloaded 09/25/19 to 130.192.92.55. Redistribution subject to SIAM license or copyright; see http://www.siam.org/journals/ojsa.php

require us to make additional assumptions on the geometry of $\Omega(z)$ that we discuss next in connection with properties of the rate function $I(\theta)$ defined in (1.7).

Letting

$$\theta^\star(z) = \operatorname*{argmin}_{\theta\in\Omega(z)} I(\theta)\,, \tag{2.7}$$

we first make the following assumption.

Assumption 3. There exists a finite z_0 such that, $\forall z \geq z_0$, $\theta^\star : [z_0, \infty) \to \Omega$ is continuously differentiable and $I(\theta^\star(\cdot))$ is strictly increasing with z with

$$I(\theta^\star(z)) \to \infty \quad \text{and} \quad |\nabla I(\theta^\star(z))| \geq K > 0 \quad \text{as} \quad z \to \infty. \tag{2.8}$$

This assumption implies that $\theta^\star(z) \in \partial\Omega(z)$ for $z > z_0$, i.e., we can replace (2.7) with

$$\theta^\star(z) = \operatorname*{argmin}_{\theta\in\partial\Omega(z)} I(\theta)\,. \tag{2.9}$$

The Euler–Lagrange equation for (2.9) is

$$\nabla I(\theta^\star(z)) = \lambda \nabla F(\theta^\star(z)) \tag{2.10}$$

for some Lagrange multiplier λ. Since by definition both S and I are convex functions, by the involution property of the Legendre transform we have

$$S(\eta) = \max_\theta \left(\langle \eta, \theta\rangle - I(\theta)\right)\,, \tag{2.11}$$

and this maximum is achieved at the solution of

$$\eta = \nabla I(\theta) \tag{2.12}$$

in θ. Therefore if we define $\eta^\star(z)$ via

$$\eta^\star(z) = \nabla I(\theta^\star(z)) \tag{2.13}$$

the mean of $\mu_{\eta^\star(z)}$ is $\theta^\star(z)$. From (2.11) this also implies that

$$\langle \eta^\star(z), \theta^\star(z)\rangle - S(\eta^\star(z)) = I(\theta^\star(z))\,, \tag{2.14}$$

which gives the following exact representation formula for $\mu(\Omega(z))$:

$$\begin{aligned} \mu(\Omega(z)) &= \int_{\Omega(z)} e^{S(\eta^\star(z)) - \langle \eta^\star(z), \theta\rangle} d\mu_{\eta^\star(z)}(\theta) \\ &= e^{-I(\theta^\star(z))} \int_{\Omega(z)} e^{-\langle \eta^\star(z), (\theta - \theta^\star(z))\rangle} d\mu_{\eta^\star(z)}(\theta)\,. \end{aligned} \tag{2.15}$$

Copyright © by SIAM and ASA. Unauthorized reproduction of this article is prohibited.

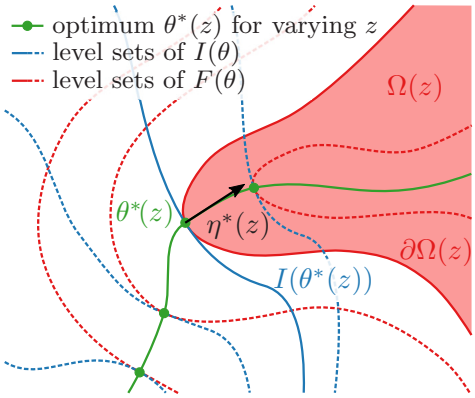

Figure 1. *Schematic interpretation of the object involved in Theorem 2.1. For a given z, $\theta^*(z)$ is the point on $\partial\Omega(z)$ that minimizes $I(\theta)$. The normal to the level set of $I(\theta)$ is $\eta^*(z) = \nabla I(\theta^*(z))$.*

For a geometric illustration of the objects introduced in (2.7)–(2.15) see Figure 1. To proceed further we need to make assumptions about $\Omega(z)$.

Assumption 4. For all $z \geq z_0$, the set $\Omega(z)$ is contained in the half-space whose boundary is tangent to $\Omega(z)$ at $\theta = \theta^\star(z)$, i.e.,

$$\Omega(z) \subseteq \mathcal{H}(z) = \{\theta \ : \langle \hat{n}^\star(z), \theta - \theta^\star(z)\rangle \geq 0\}\,, \tag{2.16}$$

where $\hat{n}^\star(z) = \nabla F(\theta^\star(z))/|\nabla F(\theta^\star(z))|$ denotes the inward pointing unit normal to $\partial\Omega(z)$ at $\theta^\star(z)$.

In the terminology of Ney [31], it means that $\theta^\star(z)$ is a dominating point in $\Omega(z)$. If we combine (2.10) and (2.13) we deduce that

$$\frac{\eta^\star(z)}{|\eta^\star(z)|} = \frac{\nabla F(\theta^\star(z))}{|\nabla F(\theta^\star(z))|} = \hat{n}^\star(z) \tag{2.17}$$

and as a result we can use Fubini's theorem to express (2.15) as

$$\mu(\Omega(z)) = e^{-I(\theta^\star(z))} \int_0^\infty e^{-|\eta^\star(z)|s} |\eta^\star(z)| G(z,s)\, ds\,. \tag{2.18}$$

Here we defined

$$G(z,s) = \mu_{\eta^\star(z)}\left(\Omega(z) \setminus \mathcal{H}(z,s)\right) \tag{2.19}$$

with

$$\mathcal{H}(z,s) = \{\theta \ : \ \langle \hat{n}^\star(z), (\theta - \theta^\star(z) - \hat{n}^\star(z)s)\rangle \geq 0\}\ . \tag{2.20}$$

Note that in (2.18) the lower limit of the integral is at $s = 0$ by Assumption 4. Since by definition we have

$$\forall s > 0 \ : \ G(z,s) \in (0,1), \quad \forall s, s' > 0,\ s' > s \ : \ G(z,s') > G(z,s), \quad \lim_{s\to 0^+} G(z,s) = 0\,, \tag{2.21}$$

Copyright © by SIAM and ASA. Unauthorized reproduction of this article is prohibited.

Downloaded 09/25/19 to 130.192.92.55. Redistribution subject to SIAM license or copyright; see http://www.siam.org/journals/ojsa.php

Downloaded 09/25/19 to 130.192.92.55. Redistribution subject to SIAM license or copyright; see http://www.siam.org/journals/ojsa.php

from (2.18) we obtain the upper bound

$$\mu(\Omega(z)) \le e^{-I(\theta^\star(z))} \int_0^\infty e^{-|\eta^\star(z)|s} |\eta^\star(z)| ds = e^{-I(\theta^\star(z))}, \tag{2.22}$$

which implies

$$\frac{\log \mu(\Omega(z))}{I(\theta^\star(z))} \le -1. \tag{2.23}$$

To get a matching lower bound notice that for all $s_1 > 0$ we have

$$\begin{aligned} \mu(\Omega(z)) &\ge e^{-I(\theta^\star(z))} \int_0^{s_1} e^{-|\eta^\star(z)|s} |\eta^\star(z)| G(z,s) ds \\ &\ge e^{-I(\theta^\star(z))} G(z,s_1) \left(1 - e^{-|\eta^\star(z)|s_1}\right) \\ &\ge e^{-I(\theta^\star(z))} G(z,s_1) \frac{|\eta^\star(z)|s_1}{1+|\eta^\star(z)|s_1}. \end{aligned} \tag{2.24}$$

To obtain a bound, we need to make the following assumption.

Assumption 5. There exists $s_1 > 0$ such that

$$\lim_{z\to\infty} \frac{\log G(z,s_1)}{I(\theta^\star(z))} = 0. \tag{2.25}$$

For this s_1 we have (using also Assumption 3 that guarantees that $|\eta^\star(z)| \ge K > 0$)

$$\begin{aligned} \frac{\log \mu(\Omega(z))}{I(\theta^\star(z))} &\ge -1 + \frac{\log G(z,s_1) + \log\left(|\eta^\star(z)|s_1\right) - \log\left(1+|\eta^\star(z)|s_1\right)}{I(\theta^\star(z))} \\ &= -1 + \frac{\log G(z,s_1) - \log\left(1+|\eta^\star(z)|^{-1}s_1^{-1}\right)}{I(\theta^\star(z))} \\ &\to -1 \qquad \text{as} \quad z\to\infty. \end{aligned} \tag{2.26}$$

Combining (2.23) and (2.26) we finally deduce the following.

Theorem 2.1 (large deviation principle). *Under Assumptions 1–5, the following result holds:*

$$\lim_{z\to\infty} \frac{\log P(z)}{I(\theta^\star(z))} = \lim_{z\to\infty} \frac{\log \mu(\Omega(z))}{I(\theta^\star(z))} = -1. \tag{2.27}$$

Note that (2.27) is just a rephrasing of (1.6).

It is useful to comment on the assumptions on $\Omega(z)$ that lead to Theorem 2.1. Assumption 3 states that the event $\{F(\vartheta) \ge z\}$ becomes rare as $z \to \infty$, which is clearly necessary for an LDP to apply. Assumption 4 guarantees that all regions in $\Omega(z)$ remain much more unlikely than $\theta^\star(z)$: this assumption can be relaxed, but at the price of having to analyze more carefully how $I(\theta)$ behaves on $\partial\Omega(z)$ and exclude that regions with lower likelihood near this boundary accumulate and eventually dominate the probability. Finally, Assumption 5 is about the shape of the set $\Omega(z)$ near $\theta^\star(z)$. Since the mean of $\mu_{\eta^\star(z)}$ is $\theta^\star(z)$, we know

Copyright © by SIAM and ASA. Unauthorized reproduction of this article is prohibited.

Downloaded 09/25/19 to 130.192.92.55. Redistribution subject to SIAM license or copyright; see http://www.siam.org/journals/ojsa.php

that this measure must have mass in a region around $\theta^\star(z)$ but we need to make sure that this region has sufficient overlap with $\Omega(z)$. For example, if for each $z \geq z_0$ we can insert in $\Omega(z)$ a set that contains $\theta^\star(z)$ on its boundary and is such that its volume remains finite as $z \to \infty$, Assumption 5 will automatically hold. On the other hand, this assumption could fail, for example, if $\Omega(z)$ becomes increasingly thin. More discussion about this kind of geometric assumption can be found, e.g., in [23, 29].

It is also interesting to note that (2.18) offers a way to derive asymptotic expansions for $\mu(\Omega(z))$ more refined than (2.27) if we assume that (i) $|\eta^\star(z)|$ grows with z, i.e., we supplement (2.8) with

$$|\eta^\star(z)| = |\nabla I(\theta^\star(z))| \to \infty \qquad \text{as} \quad z \to \infty\,, \tag{2.28}$$

and (ii) $G(z,s)$ has a specific behavior near $s=0$ as $z \to \infty$. For example, suppose that there is a $C > 0$ such that for all $u \geq 0$

$$G(z, |\eta^\star(z)|^{-1}u) \sim C|\eta^\star(z)|^{-\alpha}u^\alpha \qquad \text{with} \quad \alpha > 0 \quad \text{as} \quad z, |\eta^\star(z)| \to \infty\,, \tag{2.29}$$

where $f(z) \sim g(z)$ indicates that $\lim_{z\to\infty} f(z)/g(z) = 1$. Then we have

$$\begin{aligned} P(z) = \mu(\Omega(z)) &= e^{-I(\theta^\star(z))} \int_0^\infty e^{-u} G\left(z, |\eta^\star(z)|^{-1}u\right) du \\ &\sim e^{-I(\theta^\star(z))} C|\eta^\star(z)|^{-\alpha} \int_0^\infty e^{-u}u^\alpha du \\ &= C\Gamma(\alpha+1)|\eta^\star(z)|^{-\alpha} e^{-I(\theta^\star(z))}\,. \end{aligned} \tag{2.30}$$

It is interesting to note that both (2.18) and (2.30) are consistent with $\vartheta|_{\Omega(z)}$ (outcome of the event conditioned on $F(\vartheta) \geq z$) having fluctuations of order $O(|\eta^\star(z)|^{-1})$ away from $\theta^\star(z)$ in the direction parallel to $\eta^\star(z)$. Perpendicular to $\eta^\star(z)$ the fluctuations remain of order $O(1)$ even as $z \to \infty$, but integrating in these perpendicular directions only gives a subexponential correction to $\mu(\Omega(z))$. This correction depends on the geometry of the hypersurface $\partial\Omega(z)$ (in particular on its curvature) near $\theta^\star(z)$. This is what is accounted for in (2.30), and this picture will be confirmed in the numerical examples below.

Illustration: Gaussian measure with linear observable. Let us illustrate the LDT optimization in the simple case of a Gaussian random variable ϑ with mean 0 and covariance Id, taking values $\theta \in \mathbb{R}^N$. If we consider a linear observable

$$F(\theta) = \langle b, \theta \rangle, \qquad b \in \mathbb{R}^N\,, \tag{2.31}$$

we have

$$\mathbb{P}(\langle b, \vartheta \rangle \geq z) = (2\pi)^{-N/2} \int_{\langle b,\theta\rangle \geq z} \exp\left(-\tfrac{1}{2}|\theta|^2\right) d\theta\,, \tag{2.32}$$

and a direct calculation shows that

$$\mathbb{P}(\langle b, \theta \rangle \geq z) = \tfrac{1}{2}\operatorname{erfc}\left(\frac{z}{\sqrt{2}|b|}\right) \sim (2\pi)^{-1/2}|b|z^{-1}\exp\left(-\tfrac{1}{2}|b|^{-2}z^2\right) \quad \text{as} \quad z \to \infty\,. \tag{2.33}$$

Copyright © by SIAM and ASA. Unauthorized reproduction of this article is prohibited.

Downloaded 09/25/19 to 130.192.92.55. Redistribution subject to SIAM license or copyright; see http://www.siam.org/journals/ojsa.php

Let us check that the LDP derived above is consistent with this result. Here

$$I(\theta) = \tfrac{1}{2}|\theta|^2, \qquad S(\eta) = \tfrac{1}{2}|\eta|^2. \tag{2.34}$$

If we minimize $I(\theta)$ subject to $\langle \theta, b\rangle \geq z$, we deduce

$$\theta^\star(z) = z|b|^{-2}b \qquad \text{and} \qquad I(\theta^\star(z)) = \tfrac{1}{2}|b|^{-2}z^2. \tag{2.35}$$

Comparing this result with (2.33) we see that it is consistent with the prediction in (2.27).

We can also test what the theory can say beyond the log-asymptotic estimate. Here, the planar condition corresponding to $\Omega(z) = \mathcal{H}(z)$ is exactly fulfilled by linearity of $F(\theta) = \langle b, \theta\rangle$. We need to estimate $G(z, |\eta^\star(z)|^{-1})$ as $z \to \infty$. From (2.13) and (2.14) we have that

$$\eta^\star(z) = \nabla I(\theta^\star(z)) = \theta^\star(z) = z|b|^{-2}b, \qquad S(\eta^\star(z)) = \tfrac{1}{2}z^2|b|^{-2}\,, \tag{2.36}$$

and the tilted measure (2.4) at $\eta = \eta^\star(z)$ reads

$$d\mu_{\eta^\star(z)}(\theta) = (2\pi)^{-N/2}\exp\left(-\tfrac{1}{2}|\theta|^2 + zb|b|^{-2}\langle b, \theta\rangle - \tfrac{1}{2}z^2|b|^{-2}\right)d\theta\,. \tag{2.37}$$

Using (2.36), we obtain

$$\begin{aligned} G(z,s) &= \int_{z\leq\langle b,\theta\rangle\leq z+s} d\mu_{\eta^\star(z)}(\theta) \\ &= (2\pi)^{-1/2}\int_0^s \exp\left(-\tfrac{1}{2}u^2\right)du \\ &= \tfrac{1}{2}\operatorname{erf}\left(\tfrac{1}{2}\sqrt{2}s\right)\,. \end{aligned} \tag{2.38}$$

As a result

$$G(z, |\eta^\star(z)|^{-1}s) \sim (2\pi)^{-1/2}|\eta^\star(z)|^{-1}s = (2\pi)^{-1/2}|b|sz^{-1} \qquad \text{as} \quad z \to \infty. \tag{2.39}$$

Comparing with (2.29), we see that here $C = (2\pi)^{-1/2}$ and $\alpha = 1$. Therefore (2.30) agrees with (2.33) as expected.

3. Numerical aspects.

Here we discuss how to numerically perform the minimization in (1.6) and thereby estimate $P(z)$—the method can be straightforwardly generalized to consider also the minimization associated with the calculation of (1.3) or (1.5). We impose the constraint $f(u(T)) \geq z$ by adding a Lagrange multiplier term to (1.6), so that the minimization can be rephrased in the Hamiltonian formalism by [41, 6]

$$E(u,\theta) = I(\theta) - \lambda f(u(T)))\,, \tag{3.1}$$

where $u(T)$ should itself be viewed as a function of θ obtained by solving (1.1) with $\vartheta = \theta$, that is,

$$\partial_t u = b(u,\theta), \qquad u(t=0) = u_0(\theta). \tag{3.2}$$

The minimization of (3.1) with $u(T)$ obtained from (3.2) can be performed via steepest descent with adaptive step (line search). This requires computing the gradient of E with respect to θ, which can be achieved in two ways: by the direct and the adjoint methods [6, 35]. These steps are described next.

Copyright © by SIAM and ASA. Unauthorized reproduction of this article is prohibited.

Downloaded 09/25/19 to 130.192.92.55. Redistribution subject to SIAM license or copyright; see http://www.siam.org/journals/ojsa.php

3.1. Gradient calculation.

3.1.1. Direct method. The gradient of the cost function with respect to the control reads

$$\nabla_\theta E(u(T,\theta),\theta) = \partial_\theta E + (\partial_\theta u(T,\theta))^\top \partial_u E = \nabla_\theta I - \lambda\, J^\top(T,\theta)\, \partial_u f(u(T,\theta))\,, \tag{3.3}$$

where $J = \partial_\theta u$ is the Jacobian—componentwise $J_{i,j} = \partial u_i/\partial\theta_j$. An evolution equation for J can be obtained by differentiating (3.2) with respect to θ:

$$\partial_t J = \partial_u b\, J + \partial_\theta b, \qquad J(0) = \nabla_\theta\, u_0. \tag{3.4}$$

Summing up, given the current state of the control, θ^n, we calculate the gradient of the objective function via the following:

1. *Field estimation.* Obtain the current field u^n by solving

$$\partial_t u^n = b(u^n,\theta^n), \qquad u^n(0) = u_0(\theta^n)\,. \tag{3.5}$$

2. *Jacobian estimation.* Obtain the Jacobian J^n by solving

$$\partial_t J^n = \partial_u b(u^n,\theta^n)\, J^n + \partial_\theta b(u^n,\theta^n), \qquad J^n(0) = \nabla_\theta\, u_0(\theta^n). \tag{3.6}$$

3. *Gradient calculation.* Compute the gradient $(\nabla_\theta E)^n$ via

$$(\nabla_\theta E)^n = \nabla_\theta I(\theta^n) - \lambda\,(J^n(T))^\top\, \partial_u f(u^n(T)). \tag{3.7}$$

3.1.2. Adjoint method. Let us introduce the adjoint field $p(t)$ solution of

$$\partial_t p = -(\partial_u b)^\top p, \qquad p(T,\theta) = \lambda \partial_u f(u(T,\theta)). \tag{3.8}$$

Using this equation as well as the transpose of (3.4) we deduce

$$\begin{aligned} \partial_t(J^\top p) &= \partial_t J^\top p + J^\top \partial_t p \\ &= J^\top(\partial_u b)^\top p + (\partial_\theta b)^\top p - J^\top(\partial_u b)^\top p = (\partial_\theta b)^\top p\,. \end{aligned} \tag{3.9}$$

As a result

$$\int_0^T (\partial_\theta b)^\top p dt = J^\top(T)p(T) - J^\top(0)p(0) = \lambda J^\top(T,\theta)\partial_u f(u(T,\theta)) - (\nabla_\theta u_0)^\top p(0,\theta). \tag{3.10}$$

This expression offers a way to write the gradient of the objective function in (3.3) as

$$\nabla_\theta E = \nabla_\theta I - (\nabla_\theta u_0)^\top p(0,\theta) - \int_0^T (\partial_\theta b)^\top p\, dt\,. \tag{3.11}$$

Using this expression instead of (3.3) is computationally advantageous because it avoids the calculation of the Jacobian J—note in particular that the adjoint field p has the same dimensions as u, independent of the dimensions of the space Ω. The price to pay is the field u must be computed and stored separately since (3.8) for p must be solved backward in time. Summarizing, the gradient of the objective function is now calculated via the following:

Copyright © by SIAM and ASA. Unauthorized reproduction of this article is prohibited.

Downloaded 09/25/19 to 130.192.92.55. Redistribution subject to SIAM license or copyright; see http://www.siam.org/journals/ojsa.php

1. *Field estimation.* Obtain the current field u^n by solving

$$\partial_t u^n = b(u^n, \theta^n), \qquad u^n(0) = u_0(\theta^n). \tag{3.12}$$

2. *Adjoint field estimation.* Obtain the adjoint field p^n by solving

$$\partial_t p^n = -(\partial_u b(u^n, \theta^n))^\top p^n, \qquad p^n(T) = \lambda \partial_u f(u^n(T)). \tag{3.13}$$

3. *Gradient calculation.* Compute the gradient $(\nabla_\theta E)^n$ via

$$(\nabla_\theta E)^n = \nabla_\theta I(\theta^n) - (\nabla_\theta u_0(\theta^n))^\top p^n(0) - \int_0^T (\partial_\theta b(u^n(t), \theta^n))^\top p^n(t)\, dt\,. \tag{3.14}$$

Note that (3.12) for u and (3.13) for p are adjoint in both space and time. As a result the numerical simulation of these equations has to be done with care, as the integration scheme used for one equation needs to be the adjoint of the other. This is preferably done by using schemes that are self-adjoint. For recent literature on the topic we refer the reader to [45, 22, 44].

3.2. Descent with preconditioning of the gradient. Once we have calculated the gradient of the objective function at θ^n, we can make a downhill step in the cost function landscape using the following

4. *Descent step with pre-conditioning:*

$$\theta^{n+1} = \theta^n - \alpha^n B^n (\nabla_\theta E)^n\,, \tag{3.15}$$

where B^n is a preconditioning $M \times M$ matrix (recall that $\theta \in \Omega \subseteq \mathbb{R}^M$), and $\alpha^n > 0$ is the step size that is tuned optimally at each iteration via line search: this can be done using classical merit functions as discussed in [46].

The estimate of the matrix B^n deserves some further comments. Ideally, in the iterative Newton's method to search for the solution to $\nabla_\theta E = 0$, the stationary point, the preconditioner B^n is the inverse of the Hessian of the objective function $E(\theta^n)$, but this Hessian is typically difficult to calculate. Therefore, a simpler solution is to use the Hessian of the prior $I(\theta^n)$, which in the case of a Gaussian measure is simply the inverse covariance matrix C^{-1} (which is independent of θ). Since this estimate coincides with the Hessian of $E(\theta^n)$ only when $\lambda = 0$, it will deteriorate when λ increases and the preconditioning may become inefficient. If that is the case, it may be useful to switch to "quasi-Newton" methods such as the BFGS algorithm, or the limited-memory BFGS algorithm when M is very large (> 100). In the applications treated in this paper, the naive preconditioning depending only on the prior $I(\theta)$ turned out to be sufficient to perform the optimization efficiently.

Since we are typically interested in calculating (1.6) for a range of values of z, instead of fixing z and trying to determine the corresponding Lagrange multiplier λ in (3.3), it is easier to vary λ and determine a posteriori which value of z this leads to. Indeed this offers a parametric representation of $\theta^\star(z)$ via

$$\theta^\star(z(\lambda)) = \tilde{\theta}^\star(\lambda), \qquad z(\lambda) = f(u(T, \tilde{\theta}^\star(\lambda))\,, \tag{3.16}$$

where $\tilde{\theta}^\star(\lambda)$ is the minimizer of $E(\theta)$ at λ fixed. We can then also calculate $I(\theta^\star(z(\lambda))) = I(\tilde{\theta}^\star(\lambda))$ and estimate $P(z(\lambda)) \asymp \exp(-I(\tilde{\theta}^\star(\lambda)))$.

Copyright © by SIAM and ASA. Unauthorized reproduction of this article is prohibited.

Downloaded 09/25/19 to 130.192.92.55. Redistribution subject to SIAM license or copyright; see http://www.siam.org/journals/ojsa.php

4. Applications.

4.1. Elasticity of a heterogeneous rod. In this section we study a model for a one-dimensional rod with random elasticity coefficient subject to a prescribed external mechanical forcing (i.e., pulling at one end). This model (or generalizations thereof) may be of interest in actual applications (e.g., as a coarse-grained model of DNA stretching [8, 10, 30]). Here it is primarily used as a simple illustrative example of the tools and concepts introduced in sections 2 and 3. In particular, we use LDT to locate the most likely configurations leading to extreme responses and we show that such realizations dominate the statistics asymptotically.

For a simple linear forcing protocol, we are able to derive analytical results which are used to validate our numerical method. We also study the extreme events that occur under a nonlinear forcing, when no analytical solution is available.

4.1.1. Continuous model with random structure. Consider a one-dimensional elastic rod of length 1 that is being pulled at one end with a time-dependent force and whose energy is specified in terms of its displacement field $u : [0,1] \to \mathbb{R}$ via

$$V(u,t) = \frac{1}{2}\int_0^1 \mathcal{D}(x)\,|\partial_x u|^2\,dx - r(t)u(1)\,, \tag{4.1}$$

where the first term is the total internal energy of the rod and the second term is the external energy (negative of the work potential); $\mathcal{D}(x) > 0$ is the elasticity coefficient, assumed to be spatially dependent, and $r(t)$ is a prescribed external forcing protocol acting on the right end of the rod—the specific form of $r(t)$ will be introduced later. The dynamics of the rod is governed by the Euler–Lagrange equation associated with (4.1):

$$\partial_t^2 u = \partial_x(\mathcal{D}(x)\partial_x u), \quad x \in (0,1)\,, \tag{4.2}$$

with initial conditions to be prescribed later and boundary conditions

$$u(t,0) = 0\,, \quad \mathcal{D}(1)\partial_x u(t,1) = r(t) \quad \forall t \geq 0\,. \tag{4.3}$$

In order to introduce uncertainty in the model we make the elasticity random, i.e., we take $\mathcal{D}(x) \equiv \mathcal{D}(x,\vartheta)$. Here we will assume that $\mathcal{D}(x,\vartheta)$ is piecewise constant over blocks of size $1/M$ for some $M \in \mathbb{N}$, with independent values in each block. Specifically, we take

$$\mathcal{D}(x,\vartheta) = \sum_{k=1}^{M} \varphi_k(x) g(\vartheta_k)\,, \tag{4.4}$$

where the functions $\{\varphi_k\}_{k=1}^M$ are given by

$$\varphi_k(x) = \begin{cases} 1 & \text{if} \quad M^{-1}(k-1) \leq x < M^{-1}k\,, \\ 0 & \text{otherwise;} \end{cases} \tag{4.5}$$

g is a given function; and $\{\vartheta_k\}_{k=1}^M$ are independent and identically distributed random variables. Below we will consider two cases.

Copyright © by SIAM and ASA. Unauthorized reproduction of this article is prohibited.

Downloaded 09/25/19 to 130.192.92.55. Redistribution subject to SIAM license or copyright; see http://www.siam.org/journals/ojsa.php

Case 1. As a simple test case, assume that $g : (0, \infty) \to (0, \infty)$ with

$$g(y) = y^{-1} \tag{4.6}$$

and we take the variable $\{\vartheta_k\}_{k=1}^M$ to be exponentially distributed, i.e.,

$$\mathbb{P}(\vartheta_k \geq y) = e^{-\alpha y}, \qquad y \geq 0, \quad \alpha > 0\,. \tag{4.7}$$

This choice implies that

$$S(\eta) = \log \mathbb{E} e^{\langle \eta, \vartheta \rangle} = -\sum_{k=1}^{M} \log(1 - \alpha^{-1}\eta_k), \qquad \eta_k < \alpha \quad \forall k = 1, \ldots, M, \tag{4.8}$$

so that

$$I(\theta) = \sum_{k=1}^{M} (\alpha\theta_k - 1 - \log \theta_k) \qquad \theta_k > 0 \quad \forall k = 1, \ldots, M\,. \tag{4.9}$$

Case 2. Here we assume that $g : \mathbb{R} \to (0, \infty)$ with

$$g(y) = \tfrac{1}{2}y + \sqrt{\tfrac{1}{4}y^2 + 1}, \tag{4.10}$$

and we take the variable $\{\vartheta_k\}_{k=1}^M$ to be normally distributed with variance $\sigma^2 > 0$, i.e.,

$$\vartheta_k = \mathcal{N}(0, \sigma^2)\,. \tag{4.11}$$

For this choice, we have

$$S(\eta) = \tfrac{1}{2} \sum_{k=1}^{N} \sigma^2 \eta_k^2, \qquad I(\theta) = \tfrac{1}{2} \sum_{k=1}^{N} \sigma^{-2} \theta_k^2\,. \tag{4.12}$$

Given this random input, our aim is to investigate the statistics of the displacement of the right end of the rod at time T: this amounts to considering the observable $f(u(T)) = u(T, 1)$ and studying the behavior of

$$P(z) = \mathbb{P}(u(T, 1, \vartheta) \geq z) \qquad \text{for} \quad z \gg 1. \tag{4.13}$$

Below we will analyze the behavior of this quantity in two cases: when the forcing $r(t)$ in (4.1) is linear in t and when it is not—the first situation is amenable to analytical treatment whereas the second is not in general. Note that in both situations, the behavior of $P(z)$ for large z will depend on how fast $g(u)$ decays to zero: due to the shape of g this will depend on the right tail of the distribution of ϑ_k in Case 1 and on its left tail in Case 2.

Copyright © by SIAM and ASA. Unauthorized reproduction of this article is prohibited.

Downloaded 09/25/19 to 130.192.92.55. Redistribution subject to SIAM license or copyright; see http://www.siam.org/journals/ojsa.php

4.1.2. Discrete model. To perform the numerics, we need to consider a spatially discretized version of the model above. We do so by introducing the discrete energy

$$V(u,t) = \frac{1}{2}\sum_{j=0}^{N-1} \mathcal{D}_{j+1}(\vartheta)\frac{(u_{j+1}-u_j)^2}{\Delta x} - r(t)\,u_N\,, \tag{4.14}$$

in which $u_j = u(j\Delta x)$, $\mathcal{D}_j = \mathcal{D}(j\Delta x)$, $\Delta x = 1/N$. Alternatively, (4.14) can be thought of as the energy for a system of $N+1$ beads u_j connected by N springs with random spring constants $\mathcal{D}_j(\vartheta)$. The dynamics obeys the system of ODEs

$$\partial_t^2 u_j = \frac{\mathcal{D}_{j+1}}{\Delta x^2}(u_{j+1}-u_j) - \frac{\mathcal{D}_j}{\Delta x^2}(u_j - u_{j-1})\,, \qquad j = 1,\dots,N-1\,, \tag{4.15}$$

with fixed boundary condition $u_0 = 0$ at the left end and dynamic boundary condition

$$\partial_t^2 u_N = -\frac{\mathcal{D}_N}{\Delta x^2}(u_N - u_{N-1}) + \frac{r(t)}{\Delta x} \tag{4.16}$$

at the right end. We will pick $N = PM$ for some $P \in \mathbb{N}$, so that by our choice for $\mathcal{D}(x,\vartheta)$ in (4.4) we have

$$\mathcal{D}_j(\vartheta) = g(\vartheta_k) \qquad \text{for } \lceil j/P \rceil = k, \quad j = 1,\dots,N, \quad k = 1\dots,M. \tag{4.17}$$

Since we focus on the statistics of the observable $f(u(T)) = u_N(T) = u(T,1)$ that measures the displacement at time T of the right end point with respect to its initial position, the cost function is

$$E(u,\theta) = I(\theta) - \lambda\, u_N(T) \tag{4.18}$$

to optimize on the parameters $\{\theta_k\}_{k=1}^M$. We will minimize (4.18) using the adjoint method to compute the gradient. As shown in the appendix, the adjoint equations read

$$\partial_t^2 p_j = \frac{\mathcal{D}_{j+1}}{\Delta x^2}(p_{j+1}-p_j) - \frac{\mathcal{D}_j}{\Delta x^2}(p_j - p_{j-1})\,, \qquad j = 1,\dots,N-1\,, \tag{4.19}$$

with conditions at the boundaries given by

$$p_0(t) = 0\,, \quad \partial_t^2 p_N = -\frac{\mathcal{D}_N}{\Delta x^2}(p_N - p_{N-1})\,, \tag{4.20}$$

and final conditions

$$p_j(T) = 0, \quad \partial_t p_j(T) = \lambda\delta_{j,N}\,. \tag{4.21}$$

The gradient of the cost function can be expressed as

$$\nabla_\theta E(u(\theta),\theta) = \nabla I(\theta) - G^\top \nabla\mathcal{D}(\theta)\,, \tag{4.22}$$

where $\nabla\mathcal{D}(\theta)$ is the $N\times M$ tensor with entries $\partial\mathcal{D}_j(\theta)/\partial\theta_k$, $j = 1,\dots,N$, $k = 1,\dots,M$, and G is a vector with entries

$$G_j = \int_0^T \frac{u_j - u_{j-1}}{\Delta x}\frac{\mu_j - \mu_{j-1}}{\Delta x}\,dt\,, \qquad j = 1,\dots,N\,. \tag{4.23}$$

Copyright © by SIAM and ASA. Unauthorized reproduction of this article is prohibited.

Downloaded 09/25/19 to 130.192.92.55. Redistribution subject to SIAM license or copyright; see http://www.siam.org/journals/ojsa.php

4.1.3. Linear forcing. Assume that $r(t) = at$ for some $a > 0$ and as initial conditions for (4.2) take

$$u(0,x) = 0\,, \quad \partial_t u(0,x) = a\int_0^x \frac{dx'}{\mathcal{D}(x',\theta)} \quad \forall x \in [0,1]\,. \tag{4.24}$$

With this choice, it is easy to check that the solution to (4.2) equipped with the boundary conditions in (4.3) is

$$u(t,x,\vartheta) = at\int_0^x \frac{dx'}{\mathcal{D}(x',\vartheta)}\,. \tag{4.25}$$

Let us consider the implications of this formula in Case 1, which is suitable to derive analytical results. Equation (4.25) implies that

$$u(T,1,\vartheta) = aT\int_0^1 \frac{dx'}{\mathcal{D}(x',\vartheta)} = \frac{aT}{M}\sum_{k=1}^{M}\vartheta_k\,, \tag{4.26}$$

where we used the specific form of $\mathcal{D}(x,\vartheta)$ given in (4.4) with g given in (4.6). Note that since the discrete equivalent to the initial conditions (4.24) is

$$u_j(0) = 0, \qquad \partial_t u_j(0) = \frac{a}{M}\sum_{k=1}^{j}\theta_k\,, \tag{4.27}$$

the result (4.26) also holds for the discretized model, i.e., we have

$$u_N(T,\vartheta) = \frac{aT}{M}\sum_{k=1}^{M}\vartheta_k\,. \tag{4.28}$$

From (4.7), this implies that $u(T,1,\vartheta) = u_N(T,\vartheta)$ follows a gamma distribution with shape parameter M and rate parameter $\alpha M(aT)^{-1}$:

$$\begin{aligned} P(z) &= \int_z^\infty \frac{(\alpha M(aT)^{-1})^M y^{M-1}}{(M-1)!} e^{-\alpha M(aT)^{-1}y} dy \\ &= \frac{1}{(M-1)!}\Gamma\left(M, \alpha M(aT)^{-1}z\right)\,, \end{aligned} \tag{4.29}$$

where $\Gamma(\cdot,\cdot)$ is the upper incomplete Gamma function. When $z \gg 1$ with M fixed, (4.29) gives

$$P(z) \sim \frac{(\alpha M(aT)^{-1}z)^{M-1}}{(M-1)!} e^{-\alpha M(aT)^{-1}z}\,, \tag{4.30}$$

meaning that

$$\log P(z) \sim -\alpha M(aT)^{-1}z + (M-1)\log(\alpha M(aT)^{-1}z) - \log(M-1)!. \tag{4.31}$$

Copyright © by SIAM and ASA. Unauthorized reproduction of this article is prohibited.

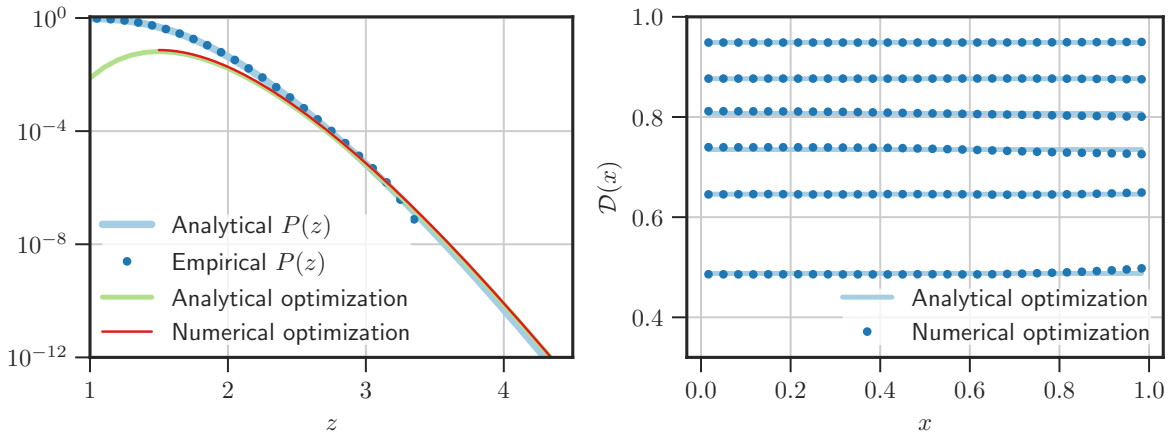

Figure 2. *Linear forcing with $a = 0.1$, final time $T = 15$, initial conditions (4.27), and the statistical prior of Case 1. The numerics are performed with $M = N = 30$. Left panel: comparison between the exact expression for $P(z)$ in (4.29), the empirical MC estimate with 2×10^7 samples, the analytical LDT estimate (4.34), and the LDT estimate obtained via numerical optimization. Right panel: comparison between the analytical (4.33) and the numerical instantons for $z = 1.58, 1.71, 1.85, 2.04, 2.32, 3.08$ from top to bottom.*

In this last expression the second and third terms at the right-hand side (RHS) are subdominant over the first, $\alpha M(aT)^{-1}z$, and disappear in the limit as $z \to \infty$. It is useful to keep these terms for comparison with the result (2.27) in Theorem 2.1 and the result (2.30), which we do next.

If we solve

$$\min I(\theta) = \min \sum_{k=1}^{M} (\alpha\theta_k - 1 - \log \alpha\theta_k) \quad \text{subject to} \quad u(T, 1, \theta) = \frac{aT}{M} \sum_{k=1}^{M} \theta_k = z\,, \tag{4.32}$$

we get

$$\theta_k^\star(z) = (aT)^{-1} z \qquad \text{for} \quad k = 1, \dots, M\,. \tag{4.33}$$

As a result

$$I(\theta^\star(z)) = M\left(\alpha(aT)^{-1}z - 1 - \log(\alpha(aT)^{-1}z)\right)\,, \tag{4.34}$$

which from (4.31) is consistent with $\log P(z) \sim -I(\theta^\star(z))$ as $z \to \infty$, as predicted by (2.27). Note also that here

$$\eta_k^\star(z) = \partial_{\theta_k} I(\theta^\star(z)) = \alpha - aTz^{-1} \qquad \text{for} \quad k = 1, \dots, M\,. \tag{4.35}$$

Since this implies that $|\eta_k^\star(z)| \to \alpha$ as $z \to \infty$, this means that the condition in (2.28) is not satisfied here.

In Figure 2 we compare the asymptotic estimate (4.34) with the exact expression (4.29). We also check that the numerical optimization is consistent with the analytical result, which is important to validate the numerical code described below.

Copyright © by SIAM and ASA. Unauthorized reproduction of this article is prohibited.

Downloaded 09/25/19 to 130.192.92.55. Redistribution subject to SIAM license or copyright; see http://www.siam.org/journals/ojsa.php

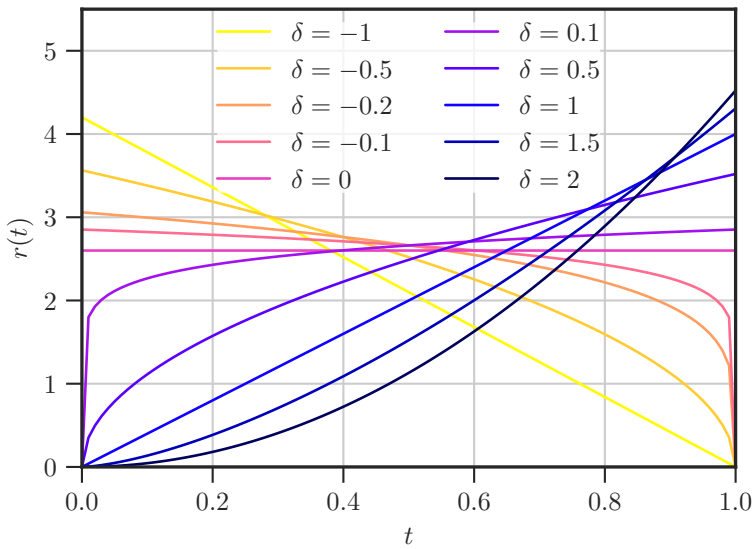

Figure 3. *The forcing protocols $r_\delta(t)$ in (4.36), which are decreasing functions of t when $\delta < 0$ and increasing functions when $\delta > 0$.*

4.1.4. Nonlinear forcing. Next we consider nonlinear forcing protocols of the type

$$r(t) = at^\beta \qquad \text{and} \qquad r(t) = a(T-t)^\beta \qquad \text{both with} \quad a, \beta > 0\,. \tag{4.36}$$

Letting $s = +1$ if $r(t) = at^\beta$ and $s = -1$ if $r(t) = a(T-t)^\beta$, we will use $r_\delta(t)$ with $\delta = s\beta$ as shorthand to describe the family of forcing protocols. They are shown in Figure 3.

As initial conditions for (4.2) we take

$$u(0,x) = 0\,, \quad \partial_t u(0,x) = 0 \quad \forall x \in [0,1]\,. \tag{4.37}$$

At discrete level these initial conditions read

$$u_j(0) = 0, \qquad \partial_t u_j(0) = 0\,. \tag{4.38}$$

In this section we restrict ourselves to Case 2 with $\sigma = 1$ and we use $M = N = 30$ and final time $T = 1$. Observing that the mean elasticity $\mathbb{E}\,(\mathcal{D}(x))$ is of order one, the average velocity of propagation of the waves along the bar is close to 1. Thus, 1 is a rough estimate of the average time that a signal takes to propagate from the right end to the left end. This means that taking $T = 1$ we are considering a short transient strongly out of equilibrium, where the random structure will contribute in a nonhomogeneous way.

To integrate (4.15) and (4.16) numerically, we use a velocity-Verlet integrator, which is of second order, symplectic, and time reversible, with a time step of 10^{-3}. The optimization is performed as described in section 3, using (4.22) and (4.23), and the iteration is terminated according to a tolerance threshold on the norm of the observed gradient of the cost function.

Copyright © by SIAM and ASA. Unauthorized reproduction of this article is prohibited.

Downloaded 09/25/19 to 130.192.92.55. Redistribution subject to SIAM license or copyright; see http://www.siam.org/journals/ojsa.php

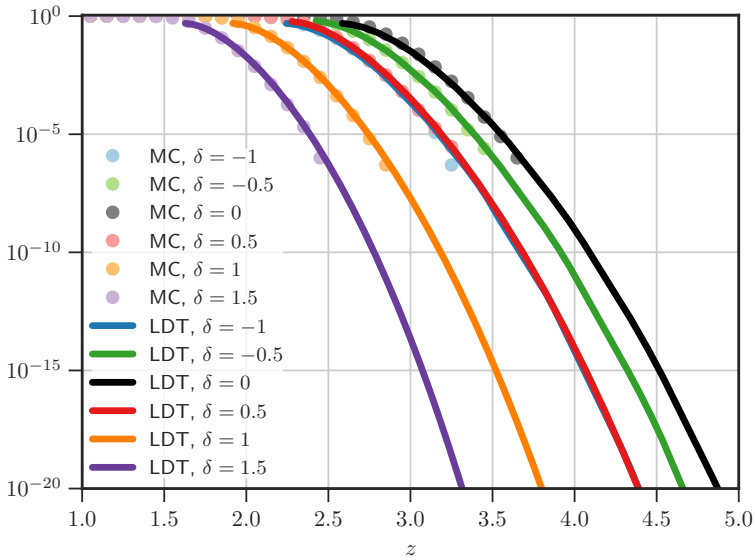

Figure 4. *Comparison between the empirical distributions $P(z)$ obtained via MC sampling and their LDT estimate. The sampling works down to events whose probability is about the inverse of the MC sampling size, while the LDT optimization allows us to extend the tails to much smaller probabilities.*

Let us now describe our results. In Figure 4 the LDT estimates of $P(z)$ are compared to the empirical estimates obtained via MC with 2×10^6 samples, showing good agreement. Next we look at the specific elasticity structure of the optimizers, $\mathcal{D}(x, \theta^\star(z))$. These are shown in Figure 5. As can be seen, the region that is relevant for having an extreme extension $u(T = 1, 1)$ occupies only the right half of the space domain, independent of the protocol. This makes sense since on average the signal takes roughly a time 1 to cross the whole domain: For a point x_0 to influence $u(T = 1, 1)$ the signal needs to have time to propagate to $x = 1$. As a result, the points on the left side will not have the possibility to influence the dynamics at all, and the optimal state of $\mathcal{D}(x, \theta)$ is determined by mere minimization of $I(\theta)$ with no dynamical constraint. In contrast, on the right side of the domain, $\mathcal{D}(x, \theta)$ must take low values to allow for large values of $u(T = 1, 1)$—since these low values are unlikely, this also accounts for the drop in probability observed in Figure 4. Figure 5 also indicates that $\mathcal{D}(x, \theta^\star(z))$ depends on the forcing protocol. This dependency can again be interpreted intuitively by realizing that the region that impacts $u(T, 1)$ the most will be the one that is reached by a strong signal (i.e., the propagation front of the most intense part of the forcing) and is able to send a strong feedback back to the right end at final time—this feedback is what is accounted for by the backward evolution of the adjoint equation in the optimization. So, the earlier the most intense part of the forcing takes place, the further from the right end a low elasticity peak appears. This explains why going toward negative δ the low-elasticity peak moves to the left in Figure 5, and the constant forcing ($\delta = 0$) is the one where the low elasticity contribution is the most uniformly distributed.

Note that in this framework it is possible to compare how likely the protocols are to produce extreme realizations of a given size, as shown in the insets in Figure 5. In this sense,

Copyright © by SIAM and ASA. Unauthorized reproduction of this article is prohibited.

Downloaded 09/25/19 to 130.192.92.55. Redistribution subject to SIAM license or copyright; see http://www.siam.org/journals/ojsa.php

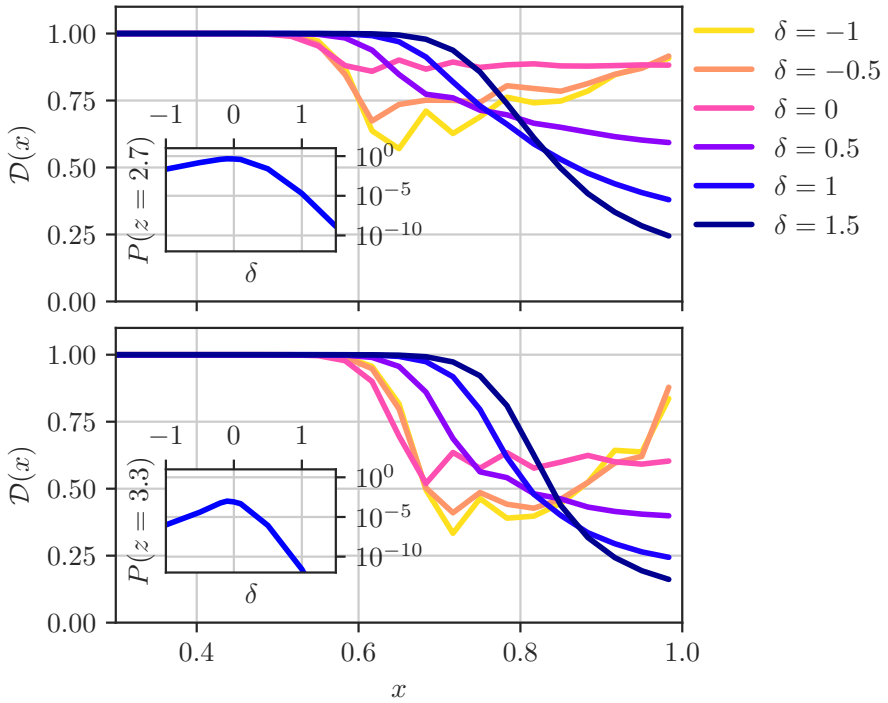

Figure 5. *Top panel: elasticity structure of the instantons for $z \geq 2.7$, for the different protocols labeled by δ. Inset: the probability $P(z = 2.7)$ as a function of the forcing protocol. Bottom panel: the same as in the top panel, but for $z \geq 3.3$. Inset: the probability $P(z = 3.3)$ as a function of δ in the forcing protocol.*

the constant protocol appears to be the optimal one. This is consistent with the fact that $\delta = 0$ is the highest curve in Figure 4.

To further clarify the role of the instantons and why they dominate the dynamics and the statistics of the extreme events, it is useful to "filter" the conditional events such that $u(T, 1) \geq z$ in the following way: First, we fix a size z and generate via MC a large set of ϑ such that $u(T, 1, \vartheta) \geq z$. Second, we average over such a conditional set to obtain the mean conditional event and its fluctuations around the mean, which is generally very close to the instanton $\theta^\star(z)$. Third, we decompose the fluctuations $\vartheta - \theta^\star(z)$ into the components parallel and perpendicular to $\eta^\star(z)$, i.e., the normal to the hypersurface $\Omega(z)$. This procedure is then repeated for various z.

In Figure 6 we show the outcome of this analysis for the protocol with $\delta = 1.5$ and for two different values of z—analogous results hold for the other kinds of forcing as well. As can be seen the average event $u(T, 1) \geq z$ lies on top of the instanton $\theta^\star(z)$, with fluctuations independent of the size of the event and also of the position along the rod (upper panels). The decomposition shows that the components perpendicular to $\eta^\star(z)$ are independent of the size of the event, and basically independent of the dynamics too. Their mean and standard deviation are the mean and the standard deviation of the unconstrained random variables ϑ (central panels). In contrast, the parallel fluctuations are small and tend to zero as z increases

Copyright © by SIAM and ASA. Unauthorized reproduction of this article is prohibited.

Downloaded 09/25/19 to 130.192.92.55. Redistribution subject to SIAM license or copyright; see http://www.siam.org/journals/ojsa.php

Downloaded 09/25/19 to 130.192.92.55. Redistribution subject to SIAM license or copyright; see http://www.siam.org/journals/ojsa.php

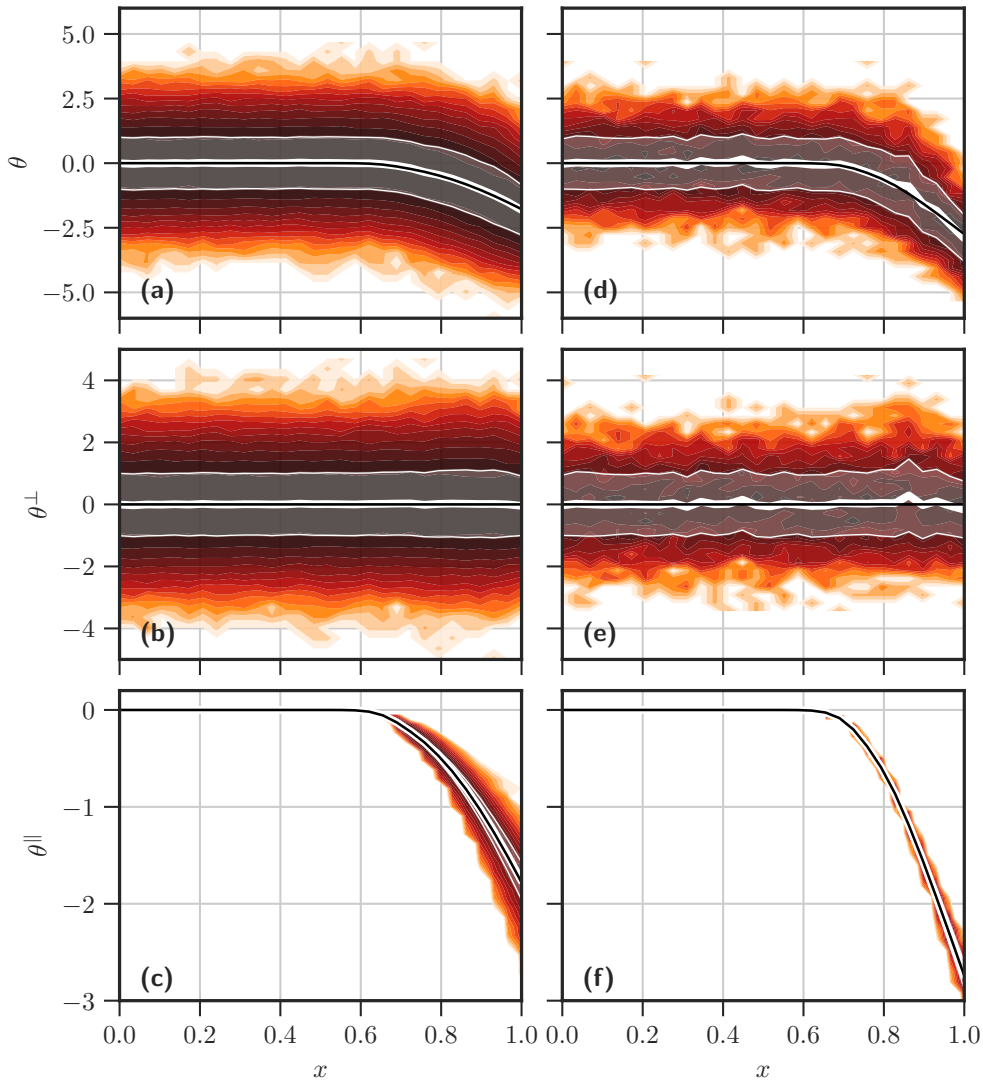

Figure 6. *Comparison between the instanton $\theta^\star(z)$ (black solid line) and the Monte Carlo sampling on the distribution of ϑ, conditioned on $u_N(1) = u(1,1) \geq z$ (color map with intensity proportional to the empirical probability density; thick white line = mean; thin white lines = one standard deviation range around the mean). Left panels: $z = 2.10$, right panels: $z = 2.40$. The top panels show the full data: the instanton agrees with the mean, but the variance does not substantially change going to more extreme events. The two central panels show the fluctuations perpendicular to $\eta^\star(z)$, confirming that their amplitude is independent of the size of the event (left and right panels have the same variance) and homogeneous in space. The bottom panels show the fluctuations in the direction parallel to $\eta^\star(z)$, indicating that their amplitude decreases as z increases, as predicted by the theory in section 2.*

(bottom panels). The scaling of the fluctuations is analyzed in more detail in Figure 7, which shows that they are $O(1)$ in the direction perpendicular to $\eta^\star(z)$ and $O(|\eta^\star(z)|^{-1})$ in the direction parallel to it, consistent with the theoretical predictions.

Copyright © by SIAM and ASA. Unauthorized reproduction of this article is prohibited.

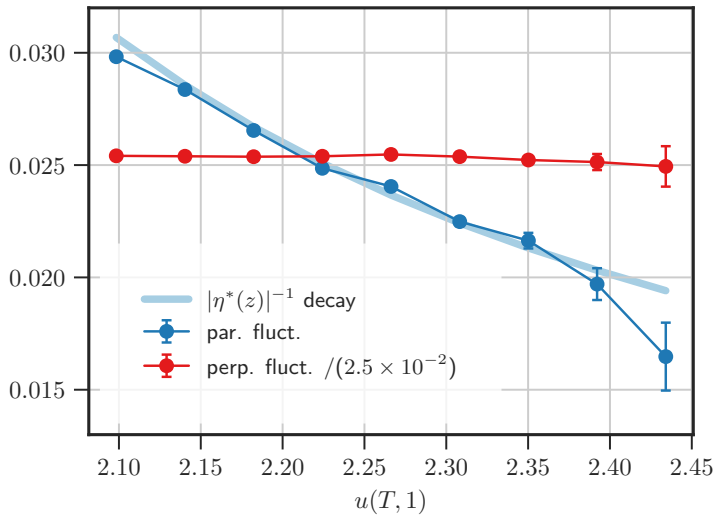

Figure 7. *Increasing z, the fluctuations in the direction perpendicular to $\eta^\star(z)$ stay constant, whereas in the parallel direction they scale as $O(|\eta^\star(z)|^{-1})$. Both behaviors are predicted analytically and here confirmed numerically. The error bars are obtained by propagating the error on the estimator of $P(z)$, which follows a Bernoulli distribution.*

4.2. Extreme events in optical turbulence.

4.2.1. The one-dimensional NLSE and the LDT formalism. The NLSE in one dimension arises in a variety of different contexts such as surface gravity waves [47, 32], nonlinear fiber optics [2], plasmas [3], and Bose–Einstein condensates [21, 34]. Here we will focus on applications of NLSE in nonlinear optics, a domain that has seen exciting experimental developments in recent years [28, 38, 40]. Specifically, we study the problem of the onset of rogue waves out of a bath of random waves taken as an initial condition for NLSE, which is a key question in *integrable turbulence* [48, 37, 1, 11, 17].

In nondimensional units, the one-dimensional NLSE for the envelope of a light beam propagating in an optical fiber reads

$$\partial_\xi \Psi = i\frac{1}{2}\partial_\tau^2 \Psi + i|\Psi|^2\Psi\,, \quad \tau \in \Gamma, \tag{4.39}$$

where $\Gamma = [0, T]$, with periodic boundary conditions $\Psi(\xi, 0) = \Psi(\xi, T)$, $\partial_\tau \Psi(\xi, 0) = \partial_\tau \Psi(\xi, T)$, and a suitable initial condition $\Psi(0, \tau) = \Psi_0(\tau)$, at the input end of the fiber $\xi = 0$. The nondimensional distance ξ, time τ, and envelope Ψ are related to the respective physical quantities x, t, and ψ via characteristic constants that depend on the specifics of the optical fiber:

$$x = \mathcal{L}_0 \xi, \qquad t = \mathcal{T}_0 \tau, \qquad \psi = \sqrt{\mathcal{P}_0}\Psi. \tag{4.40}$$

For instance, if we pick $\mathcal{T}_0 = 5$ ps, $\mathcal{L}_0 = 0.5$ km, $\mathcal{P}_0 = 0.5$ mW, the NLSE (4.39) models an optical fiber with dispersion $|\beta_2| = \mathcal{T}_0^2/\mathcal{L}_0 = 50$ ps^{2}km^{-1} and nonlinearity $\gamma = 1/(\mathcal{L}_0\mathcal{P}_0) = 4$ km^{-1}mW^{-1}.

Copyright © by SIAM and ASA. Unauthorized reproduction of this article is prohibited.

Downloaded 09/25/19 to 130.192.92.55. Redistribution subject to SIAM license or copyright; see http://www.siam.org/journals/ojsa.php

Downloaded 09/25/19 to 130.192.92.55. Redistribution subject to SIAM license or copyright; see http://www.siam.org/journals/ojsa.php

Let us denote by $\{\hat{\Psi}_n\}_{n\in\mathbb{Z}}$ the Fourier component of $\{\Psi(\tau)\}_{\tau\in[0,T]}$, i.e.,

$$\hat{\Psi}_n = \frac{1}{T}\int_0^T e^{-i\omega_n\tau}\Psi(\tau)d\tau, \qquad \Psi(\tau) = \sum_{n=-\infty}^{+\infty} e^{i\omega_n\tau}\hat{\Psi}_n\,, \tag{4.41}$$

where $\omega_n = 2\pi n/T$ and $n \in \mathbb{Z}$. Equation (4.39) is derived under the *quasi-monochromatic* assumption, meaning that the spectrum of realizations $\Psi(\tau)$ must be narrow. We ensure this with high probability by choosing a narrow power spectrum $\hat{C}_n$ defined as

$$\hat{C}_n = \frac{1}{T}\int_0^T e^{-i\omega_n\tau}C(\tau)d\tau\,, \qquad C(\tau-\tau') = \mathbb{E}(\Psi_0(\tau)\bar{\Psi}_0(\tau'))\,. \tag{4.42}$$

Here and in the following the bar denotes complex conjugation. We will consider a Gaussian spectrum with

$$\hat{C}_n = \mathcal{A}e^{-\omega_n^2/(2\Delta)} \qquad \mathcal{A} > 0, \qquad \Delta > 0, \qquad -M \le n \le M, \quad M > 0, \tag{4.43}$$

and $\hat{C}_n = 0$ for $|n| > M$. Assuming that the initial $\Psi(0,\tau)$ is a Gaussian field with mean zero and covariance $C(\tau-\tau')$, a typical set-up of statistical nonlinear optics [33, 38], this implies the representation

$$\Psi(0,\tau,\vartheta) = \sum_{n=-M}^{M} e^{i\omega_n\tau}\hat{C}_n^{1/2}\vartheta_n, \tag{4.44}$$

where ϑ_n are complex Gaussian variables with mean zero and covariance $\mathbb{E}\vartheta_n\bar{\vartheta}_m = \delta_{m,n}$, $\mathbb{E}\vartheta_n\vartheta_m = \mathbb{E}\bar{\vartheta}_n\bar{\vartheta}_m = 0$. Note that the spectral amplitude is related to the optical power $P(\xi,\tau) = |\psi(\xi,\tau)|^2$ (statistically homogeneous in τ) via $\mathcal{A} = \mathbb{E}(P)/\sum_n e^{-\omega_n^2/(2\Delta)}$. The initial statistical state of the system is thus completely determined given the two parameters Δ and $\mathbb{E}(P)$, and the average power $\mathbb{E}(P)$ is relevant to optical experiments—it also enjoys the property of being invariant under the NLSE evolution in the variable ξ, i.e., it can be measured at the input or at the output of the optical fiber, equivalently.

In the set-up above, we will investigate extreme fluctuations of the optical power at the output of the optical fiber ($\xi = L$). Recalling that $|\Psi(L,\tau)| = \sqrt{P(L,\tau)}$, this amounts to looking at the statistics of

$$f(\Psi(\vartheta)) = \max_{\tau\in\Gamma}|\Psi(L,\tau,\vartheta)|\,, \qquad L > 0. \tag{4.45}$$

Analyzing this observable using the framework developed in sections 2 and 3 amounts to minimizing the cost function (this is (3.1))

$$E(\Psi,\theta) = I(\theta) - \lambda f(\Psi) \qquad \text{with} \qquad I(\theta) = \tfrac{1}{2}\sum_{n=-M}^{M}|\theta_n|^2\,. \tag{4.46}$$

This minimization must be performed on the $2\times(2M+1)$-dimensional space $\Omega \subseteq \mathbb{C}^{2M+1}$ of the initial conditions. The gradient of the cost function (4.46) is given by

$$\nabla_\theta E(\Psi(\theta),\theta) = \nabla_\theta I(\theta) + \Re(J(L,\tau_*))^T\frac{\Re(\Psi(L,\tau_*))}{|\Psi(L,\tau_*)|} + \Im(J(L,\tau_*))^T\frac{\Im(\Psi(L,\tau_*))}{|\Psi(L,\tau_*)|}\,, \tag{4.47}$$

Copyright © by SIAM and ASA. Unauthorized reproduction of this article is prohibited.

Downloaded 09/25/19 to 130.192.92.55. Redistribution subject to SIAM license or copyright; see http://www.siam.org/journals/ojsa.php

where $\Psi(L,\tau_*) \equiv \max_{\tau\in\Gamma} |\Psi(L,\tau)|$. The field Ψ is evolved with (4.39) and the initial condition depends on the point $\theta \in \Omega$ through the mapping $\Psi(0,\theta)$ defined in (4.44), with the difference that here θ is no longer random. The matrix J (also complex) evolves according to

$$\partial_\xi J(\xi,\tau) = \int_0^L d\xi' \left(\frac{\delta b(\Psi(\xi))}{\delta\Psi(\xi')} J(\xi',\tau) + \frac{\delta b(\Psi(\xi))}{\delta\bar{\Psi}(\xi')} \bar{J}(\xi',\tau) \right), \tag{4.48}$$

where $b(\Psi(\xi)))$ is a shorthand for the RHS of (4.39): explicitly

$$\int_0^L d\xi' \frac{\delta b(\xi)}{\delta\Psi(\xi')} J(\xi') = \left(\frac{i}{2}\partial_\tau^2 + 2i|\Psi(\xi)|^2 \right) J(\xi), \tag{4.49}$$

$$\int_0^L d\xi' \frac{\delta b(\xi)}{\delta\bar{\Psi}(\xi')} \bar{J}(\xi') = i\big(\Psi(\xi)\big)^2 J(\xi). \tag{4.50}$$

The initial condition for (4.48) is

$$J(\xi=0,\theta) = \nabla_\theta \Psi(0,\theta). \tag{4.51}$$

Before turning to the results, let us explain how the numerical simulations were performed. Equations (4.39) and (4.48) were evolved from $\xi = 0$ to $\xi = L$ (up to $L = 0.2$) using the pseudospectral second order Runge–Kutta exponential-time-differencing method (ETDRK2) [12, 27] with step $d\xi = 5 \times 10^{-4}$ on a periodic box $[0,T]$ discretized by 2^{12} equidistant grid points. The size $T = 30$ is found large enough for the boundary conditions to not affect the statistics on the spatio-temporal scales considered. Each Monte Carlo simulation involves 10^6 realizations of the random initial data constructed via (4.44), with $M = 45$. Adding more modes to the initial condition does not affect the results in any significant way. The minimization was performed in the space Ω (with high dimension $2 \times (2M+1) = 182$). This step was carried out via steepest descent with adaptive step (line search) and preconditioning of the gradient, using the covariance of the initial condition as metric, as explained in section 3.

4.2.2. Results. For generality, we present the results for the normalized field $A(\xi,\tau) = \Psi(\xi,\tau)/\sqrt{\mathbb{E}(P)}$ using nondimensional units. One can easily obtain the physical dimensions by applying the straightforward transformations given in (4.40). Four sets of parameters have been chosen to explore different regimes: In Set 1, we take $\Delta = \pi$, $\mathbb{E}(P) = 5/4$; in Set 2, $\Delta = \pi/2$, $\mathbb{E}(P) = 5/4$; in Set 3, $\Delta = 3\pi/2$, $\mathbb{E}(P) = 5/4$; and in Set 4, $\Delta = \pi$, $\mathbb{E}(P) = 5/9$.

In Figure 8, the path of occurrence of two extreme events is shown for Set 1, selected among the events in the random sampling with maximum power amplification $|A|^2 = P/\mathbb{E}(P)$ exceeding a value of 40. These paths are compared to the instanton obtained by LDT optimization. Since there have been recent claims, supported by both numerical and experimental evidence [38, 40], about the universality of the Peregrine soliton (PS) as a pathway to optical rogue waves out of a random background, the PS reaching the same power amplification as the instanton is also plotted.

In Figure 9 the probability $P(z) = \mathbb{P}(\max_\tau |A(L,\tau)| \geq z)$ is shown for various values of L, showing good agreement between the results from MC sampling and those from

Copyright © by SIAM and ASA. Unauthorized reproduction of this article is prohibited.

Downloaded 09/25/19 to 130.192.92.55. Redistribution subject to SIAM license or copyright; see http://www.siam.org/journals/ojsa.php

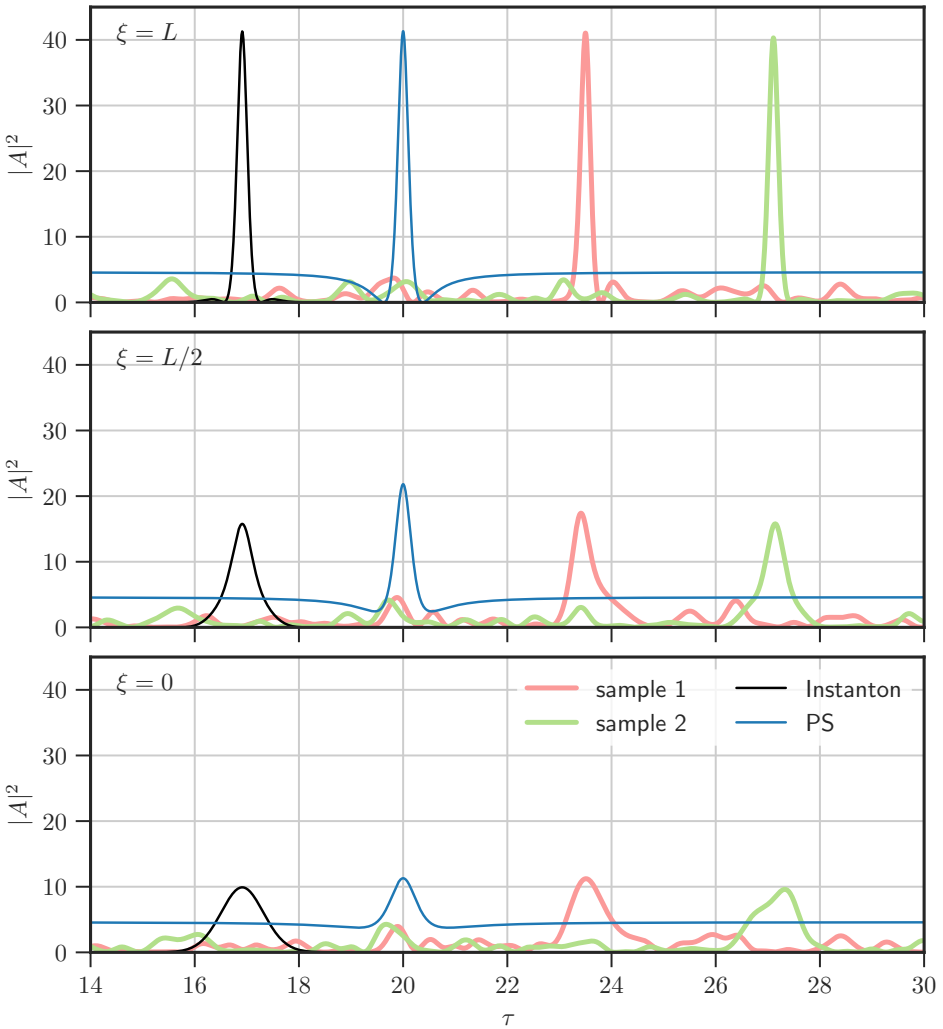

Figure 8. *Set* 1: *The paths of occurrence of two extreme events plotted are compared with the instanton and the PS reaching the same maximum power at $\xi = L$. Shown is the quantity $|A(\xi,\tau)|^2$, i.e., the power in units of average power, at three different locations ($L = 0.2$). The solution are shifted away from one another for clarity, exploiting homogeneity in τ.*

LDT optimization. A rough estimate for the onset threshold of optical rogue waves is $|A|_{RW} = 4\sqrt{2/\pi}\mathbb{E}(|A|) \simeq 2.8$ [16], independently of the set considered because of the use of the normalized variable A. As can be seen, the focusing NLSE increases the probability of large excursions of $|A(L,\tau)|$ compared to its initial Gaussian value with expectation $\mathbb{E}(|A(L=0,\tau)|) = \sqrt{\pi/4}$. This happens gradually as the distance L separating the input from the output increases. The tail fattening can be interpreted quantitatively in terms of the typical lengths of the coherent structures of NLSE. Defining the linear length as $L_{\text{lin}} = 2/\Delta^2$ and the nonlinear length as $L_{\text{nlin}} = 1/\mathbb{E}(P)$, the typical length of emergence of a PS-like structure starting from a small hump is $L_c = \frac{1}{2}\sqrt{L_{\text{lin}}L_{\text{nlin}}}$ [40]. This gives $L_c = 0.2$ for Set 1,

Copyright © by SIAM and ASA. Unauthorized reproduction of this article is prohibited.

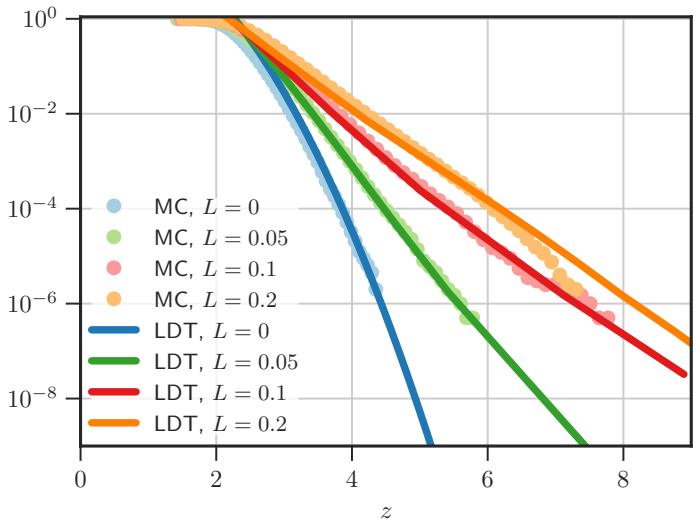

Figure 9. *Set* 1: *Comparison between the probability distributions of* $\max_\tau |A(L,\tau)|$ *in the periodic time window* $[0,T]$ *obtained by MC with* 10^6 *samples, and their corresponding LDT estimates computed using the optimization method. The plot captures the tail fattening due to the NLSE dynamics, as the output point is taken at increasing distance* L *from the input. The rogue-wave threshold is* $|A|_{RW} \simeq 2.8$. *The characteristic length of emergence of the coherent structures is* $L_c = 0.2$, *compatible with the observed tail fattening.*

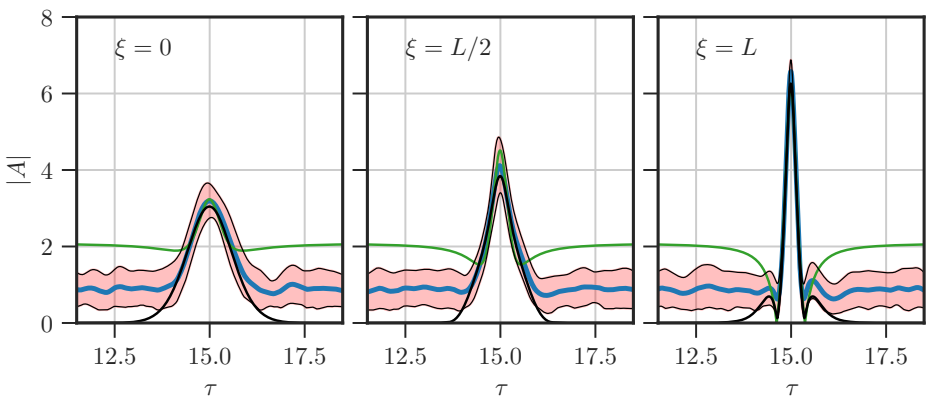

Figure 10. *Set* 1: *Results of the conditioning on the sampling for* $\max_{\tau\in\Gamma} |A(L,\tau)| \geq z = 6.25$ *with* $L = 0.2$. *Shown is the average of the conditional event (blue line), surrounded by the one standard deviation range (red area). The instanton (black line) is the optimal event reaching maximal intensity* $A = z$ *at the output point* $\xi = L$. *The PS is also represented (green line), normalized to have intensity* z *at the point of maximal space-time focusing. From left to right, the panels are at* $\xi = 0$, $\xi = L/2$, *and* $\xi = L$.

in good agreement with the width of the spatial transient over which the fast tail fattening takes place.

The asymptotic agreement of the probabilities shown in Figure 9 is numerical evidence that the focusing NLSE (4.39) with random initial data (4.44) satisfies an LDP. Additional support for the LDP is found in Figure 10, where we compare the instanton with the sam-

Copyright © by SIAM and ASA. Unauthorized reproduction of this article is prohibited.

Downloaded 09/25/19 to 130.192.92.55. Redistribution subject to SIAM license or copyright; see http://www.siam.org/journals/ojsa.php

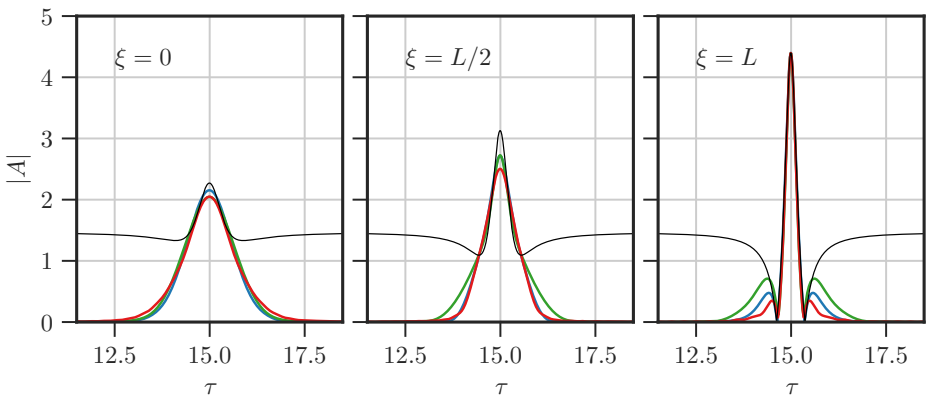

Figure 11. *Snapshots at increasing spatial coordinate from left to right ($\xi = 0$, $\xi = 0.1$, $\xi = 0.2$) of instantons reaching the same peak intensity, for the three sets of parameters with different spectral width: Set 1 ($\Delta = \pi$) in red; Set 2 ($\Delta = \pi/2$) in green; and Set 3 ($\Delta = 3\pi/2$) in blue. The PS reaching the same final height (at the point of maximal focusing) is also plotted in black. For all the profiles, striking agreement is observed around the point of maximal focusing in space-time, while significant differences are observed away from that point.*

pling mean. Looking at the signal to noise ratio, one sees that the events reaching a certain extreme amplification are all very similar. According to the results in section 2, these events are expected to have typical fluctuations in the direction perpendicular to the instanton in the space Ω: notice how away from the focusing region (determined by the direction perpendicular to the instanton because there the instanton is vanishing) the observable $|A|$ fluctuates with standard deviation $\sqrt{\mathbb{E}(P)/2}\sqrt{(4-\pi)/2}/\sqrt{\mathbb{E}(P)} \simeq 0.57$ around the expected value $\sqrt{\pi/2}\sqrt{\mathbb{E}(P)/2}/\sqrt{\mathbb{E}(P)} \simeq 0.89$, exactly as expected for typical events. Instead, the extreme size of the event is due to the component parallel to the instanton in Ω, with small fluctuations in this direction: In fact, in the focusing region (determined by the component parallel to the instanton), the signal to noise ratio becomes very big, meaning that, as z increases, the extreme rogue waves with $\max_\tau |A(\tau, L)| \geq z$ become closer to the instanton reaching $\max_\tau |A(\tau, L)| = z$. Figures 8 and 10 confirm that the high-power pulses arising spontaneously from a random background tend to the shape of the PS around its maximum space-time concentration [40]. Interpreting this in light of the gradient-catastrophe regularization [4], it is clear that such a characteristic shape of the extreme power amplifications is independent of the solitonic content of the field, although it is shared with the local behavior of an exact solitonic solution. The random extreme realizations quickly diverge from the PS away from the maximum, however. In contrast, the instantons characterize all the essential dynamics of the extreme events in integrable turbulence. They give an approximation of the extreme excursions that is much more accurate than the PS, as can be observed in Figure 10, and their shape adapts to the size of the event. In addition, unlike the PS, they come with probabilistic information and allow the estimation of the distribution tail, as seen in Figure 9, with mathematical justification in the LDT result (2.27). Furthermore, the instantons depend on the statistical state of the random background, as shown in Figure 11, while the PS is always the same. Because of these properties and their connection with the gradient catastrophe

Downloaded 09/25/19 to 130.192.92.55. Redistribution subject to SIAM license or copyright; see http://www.siam.org/journals/ojsa.php

Copyright © by SIAM and ASA. Unauthorized reproduction of this article is prohibited.

Downloaded 09/25/19 to 130.192.92.55. Redistribution subject to SIAM license or copyright; see http://www.siam.org/journals/ojsa.php

(which is their generating mechanism), the instantons can be important objects for further investigations in integrable turbulence. In this context, recent results [13] suggest that the formation of extreme coherent structures may not necessarily be linked to integrability, but may pertain to a more general class of systems with instabilities (e.g., due to nonresonant interactions) leading to spatio-temporal concentration phenomena.

5. Conclusions. We have shown that concepts from LDT, combined with optimization tools from optimal control, can be used to analyze rare events in the context of dynamical systems subject to random input in their parameters and/or their initial conditions. In our examples, the predictions from LDT were actually valid in a wide region of parameter space. This means that the large deviation regime is attained for events that are rare but still quite frequent, and extend down to extremely low probabilities, exploring regions unattainable through brute-force MC sampling. In addition, the instantons provide us with information about the mechanism of the events that can only be extracted from MC sampling via nontrivial filtering. Under this light, the LDT method stands as a competitive alternative, or at least a useful complement, to brute-force MC.

Appendix A. Calculations of section 4.1. Using the convention that $\mathcal{D}_{N+1} = 0$, the evolution equation (4.15) can be rewritten as a system of first order ODEs,

$$\begin{cases} \partial_t u_j = v_j \,, \\ \partial_t v_j = \dfrac{\mathcal{D}_{j+1}}{\Delta x^2}(u_{j+1} - u_j) - \dfrac{\mathcal{D}_j}{\Delta x^2}(u_j - u_{j-1}) + \delta_{j,N}\dfrac{r(t)}{\Delta x} \,, \end{cases} \qquad j = 1, \dots, N \,, \tag{A.1}$$

with fixed boundary condition in the origin,

$$u_0(t) = 0 \,, \tag{A.2}$$

and initial conditions

$$u_j(0) = 0, \quad v_j(0) = 0 \,. \tag{A.3}$$

To make the notation compact, we will use

$$X = \begin{pmatrix} u \\ v \end{pmatrix}, \quad Y = \begin{pmatrix} q \\ p \end{pmatrix}, \tag{A.4}$$

column vectors in $\mathbb{R}^{2N}$. Then, (A.1) can be written as

$$\partial_t X = b(X, \theta) \,, \tag{A.5}$$

where $b(X, \theta)$ is the $2N$-dimensional vector with the components of the RHS of (A.1). Note that (A.5) is in the general form (3.2) (linear system of ODEs), and this is helpful to make direct contact with the formulas (3.8) and (3.11), and thereby compute the gradient of the cost function (4.18) as

$$\nabla_\theta E = \nabla_\theta I(\theta) - \int_0^T (\partial_\theta b)^\top Y \, dt \tag{A.6}$$

Copyright © by SIAM and ASA. Unauthorized reproduction of this article is prohibited.

with Y the adjoint field to X. Let us start by deriving the adjoint equation. One can easily check that the linearization of the operator $b(X,\theta)$ for small variations of X reads

$$\partial_X b(\theta) = \begin{pmatrix} 0 & \mathrm{Id} \\ B(\theta) & 0 \end{pmatrix}, \quad \text{with} \quad B_{jk} = \frac{\mathcal{D}_{j+1}}{\Delta x^2}(\delta_{j+1,k} - \delta_{j,k}) - \frac{\mathcal{D}_j}{\Delta x^2}(\delta_{j,k} - \delta_{j-1,k}). \tag{A.7}$$

Id is the $N \times N$ identity matrix and we recall that $\mathcal{D}_j = \mathcal{D}(\theta_j)$, by (4.10). It is the adjoint operator $(\partial_X b)^\top$ that we need to compute, defined implicitly by the identity

$$\left\langle (\partial_X b)^\top Y, X' \right\rangle_{\mathbb{R}^{2N}} = \langle Y, \partial_X b\, X' \rangle_{\mathbb{R}^{2N}} \,, \tag{A.8}$$

where $\langle \cdot, \cdot \rangle_{\mathbb{R}^{2N}}$ denotes the standard scalar product in $\mathbb{R}^{2N}$. Using (A.8) we obtain

$$\begin{aligned} \langle Y, \partial_X b\, X' \rangle_{\mathbb{R}^{2N}} &= \sum_{j=1}^{N} \left(q_j v_j' + p_j \left(\frac{\mathcal{D}_{j+1}}{\Delta x^2}(u_{j+1}' - u_j') - \frac{\mathcal{D}_j}{\Delta x^2}(u_j' - u_{j-1}') \right) \right) \\ &= \sum_{j=1}^{N} \left(q_j v_j' + \left(\frac{\mathcal{D}_{j+1}}{\Delta x^2}(p_{j+1} - p_j) - \frac{\mathcal{D}_j}{\Delta x^2}(p_j - p_{j-1}) \right) u_j' \right) , \end{aligned} \tag{A.9}$$

where in the last passage we just reorganized the indices in the sum in an equivalent way, provided that we assume the boundary condition

$$p_0(t) = 0\,. \tag{A.10}$$

Comparing the last line of (A.9) with the LHS of (A.8), we deduce that

$$(\partial_X b)^\top = \begin{pmatrix} 0 & B(\theta) \\ \mathrm{Id} & 0 \end{pmatrix}, \tag{A.11}$$

which is the transpose of the RHS of (A.7) ($B(\theta)$ is symmetric), as we should expect. However, starting from the identity (A.8) is the rigorous way to obtain the adjoint operator, making the proper boundary conditions arise naturally. Plugging the result (A.11) into (3.8), we finally obtain the adjoint equation

$$\begin{cases} \partial_t q_j = \dfrac{\mathcal{D}_{j+1}}{\Delta x^2}(p_{j+1} - p_j) - \dfrac{\mathcal{D}_j}{\Delta x^2}(p_j - p_{j-1})\,, \\ \partial_t p_j = q_j\,, \end{cases} \quad j = 1, \dots, N\,, \tag{A.12}$$

with boundary condition (A.10). To obtain the correct conditions at final time, it is sufficient to observe that the final conditions of (3.8) now read

$$q_j(T) = \lambda \partial_{u_j} f(u(T)) = \lambda \delta_{j,N}\,, \qquad p_j(T) = 0. \tag{A.13}$$

Let us now compute $(\partial_\theta b)^\top$, again starting from the definition of the adjoint operator:

$$\left\langle (\partial_\theta b)^\top Y, w \right\rangle_{\mathbb{R}^N} = \langle Y, \partial_\theta b\, w \rangle_{\mathbb{R}^{2N}} \,, \tag{A.14}$$

Copyright © by SIAM and ASA. Unauthorized reproduction of this article is prohibited.

Downloaded 09/25/19 to 130.192.92.55. Redistribution subject to SIAM license or copyright; see http://www.siam.org/journals/ojsa.php

where $w \in \mathbb{R}^N$ and

$$(\partial_\theta b) = \begin{pmatrix} 0 \\ \nabla_\theta B(\theta) \end{pmatrix} \quad (\text{two } N \times N \text{ blocks}),$$
$$(\nabla_\theta B)_{jk} = \frac{\mathcal{D}'(\theta_{j+1})}{\Delta x^2}(u_{j+1} - u_j)\delta_{j+1,k} - \frac{\mathcal{D}'(\theta_j)}{\Delta x^2}(u_j - u_{j-1})\delta_{j,k}. \tag{A.15}$$

With the convention that $\mathcal{D}'(\theta_{N+1} = 0)$, a straightforward calculation yields

$$\begin{aligned} \langle Y, \partial_\theta b\, w\rangle_{\mathbb{R}^{2N}} &= \sum_{j=1}^{N} p_j \left(\frac{\mathcal{D}'(\theta_{j+1})}{\Delta x^2}(u_{j+1} - u_j)w_{j+1} - \frac{\mathcal{D}'(\theta_j)}{\Delta x^2}(u_j - u_{j-1})w_j \right) \\ &= \sum_{j=1}^{N} \left(\frac{\mathcal{D}'(\theta_j)}{\Delta x^2}(u_j - u_{j-1})(p_j - p_{j-1}) \right) w_j\,, \end{aligned} \tag{A.16}$$

from which, comparing with the LHS of (A.14), we observe that

$$((\partial_\theta b)^T Y)_j = \mathcal{D}'(\theta_j)\frac{u_j - u_{j-1}}{\Delta x}\frac{p_j - p_{j-1}}{\Delta x}\,. \tag{A.17}$$

Now, integrating in time according to (A.6),

$$\int_0^T ((\partial_\theta b)^\top Y)_j dt = \mathcal{D}'(\theta_j)\int_0^T \frac{u_j - u_{j-1}}{\Delta x}\frac{p_j - p_{j-1}}{\Delta x} dt \tag{A.18}$$

leads to (4.22).

Acknowledgments. We thank Georg Stadler for useful comments regarding the optimization method, and Gilles Francfort for suggesting the elastic rod application. We are also grateful to Lamberto Rondoni, Themis Sapsis, Freddy Bouchet, Hugo Touchette, and Pierre Suret for interesting discussions.

REFERENCES

[1] D. S. Agafontsev and V. E. Zakharov, *Integrable turbulence and formation of rogue waves*, Nonlinearity, 28 (2015), 2791.

[2] N. Akhmediev, J. M. Dudley, D. R. Solli, and S. K. Turitsyn, *Recent progress in investigating optical rogue waves*, J. Optics, 15 (2013), 060201.

[3] H. Bailung, S. K. Sharma, and Y. Nakamura, *Observation of Peregrine solitons in a multicomponent plasma with negative ions*, Phys. Rev. Lett., 107 (2011), 255005.

[4] M. Bertola and A. Tovbis, *Universality for the focusing nonlinear Schrödinger equation at the gradient catastrophe point: rational breathers and poles of the tritronquée solution to Painlevé* I, Comm. Pure Appl. Math., 66 (2013), pp. 678–752.

[5] A. A. Borovkov and B. A. Rogozin, *On the multi-dimensional central limit theorem*, Theory Probab. Appl., 10 (1965), pp. 55–62, https://doi.org/10.1137/1110005.

[6] A. Borzì and V. Schulz, *Computational Optimization of Systems Governed by Partial Differential Equations*, Comput. Sci. Eng. 8, SIAM, Philadelphia, 2011.

[7] M. Broniatowski and A. Fuchs, *Tauberian theorems, Chernoff inequality, and the tail behavior of finite convolutions of distribution functions*, Adv. Math., 116 (1995), pp. 12–33.

Copyright © by SIAM and ASA. Unauthorized reproduction of this article is prohibited.

Downloaded 09/25/19 to 130.192.92.55. Redistribution subject to SIAM license or copyright; see http://www.siam.org/journals/ojsa.php

[8] C. Bustamante, J. F. Marko, E. D. Siggia, and S. Smith, *Entropic elasticity of lambda-phage DNA*, Science, 265 (1994), pp. 1599–1599, https://doi.org/10.1126/science.8079175.

[9] F. Cérou and A. Guyader, *Adaptive multilevel splitting for rare event analysis*, Stoch. Anal. Appl., 25 (2007), pp. 417–443.

[10] P. Cluzel, A. Lebrun, C. Heller, R. Lavery, J.-L. Viovy, D. Chatenay, and F. Caron, *DNA: an extensible molecule*, Science, 271 (1996), pp. 792–794.

[11] W. Cousins and T. P. Sapsis, *Reduced-order precursors of rare events in unidirectional nonlinear water waves*, J. Fluid Mech., 790 (2016), pp. 368–388, https://doi.org/10.1017/jfm.2016.13.

[12] S. M. Cox and P. C. Matthews, *Exponential time differencing for stiff systems*, J. Comput. Phys., 176 (2002), pp. 430–455, https://doi.org/10.1006/jcph.2002.6995.

[13] G. Dematteis, T. Grafke, and E. Vanden-Eijnden, *Rogue waves and large deviations in deep sea*, Proc. Natl. Acad. Sci. USA, 115 (2018), pp. 855–860.

[14] A. Dembo and O. Zeitouni, *Large Deviations Techniques and Applications. Corrected Reprint of the Second Edition*, Stoch. Model. Appl. Probab., 38, Springer, Berlin, 2010.

[15] U. Einmahl and J. Kuelbs, *Dominating points and large deviations for random vectors*, Probab. Theory Related Fields, 105 (1996), pp. 529–543.

[16] R. El Koussaifi, A. Tikan, A. Toffoli, S. Randoux, P. Suret, and M. Onorato, *Spontaneous emergence of rogue waves in partially coherent waves: A quantitative experimental comparison between hydrodynamics and optics*, Phys. Rev. E, 97 (2018), 012208.

[17] M. Farazmand and T. P. Sapsis, *A Variational Approach to Probing Extreme Events in Turbulent Dynamical Systems*, preprint, https://arxiv.org/abs/1704.04116, 2017.

[18] U. Frisch and D. Sornette, *Extreme deviations and applications*, J. Phys. I, 7 (1997), pp. 1155–1171.

[19] C. Giardina, J. Kurchan, V. Lecomte, and J. Tailleur, *Simulating rare events in dynamical processes*, J. Stat. Phys., 145 (2011), pp. 787–811.

[20] P. Glasserman, P. Heidelberger, P. Shahabuddin, and T. Zajic, *Multilevel splitting for estimating rare event probabilities*, Oper. Res., 47 (1999), pp. 585–600.

[21] E. P. Gross, *Structure of a quantized vortex in boson systems*, Nuovo Cimento, 20 (1961).

[22] W. W. Hager, *Runge-Kutta methods in optimal control and the transformed adjoint system*, Numer. Math., 87 (2000), pp. 247–282.

[23] M. Iltis, *Sharp asymptotics of large deviations in* $\mathbb{R}^d$, J. Theoret. Probab., 8 (1995), pp. 501–522.

[24] M. Iltis, *Sharp asymptotics of large deviations for general state-space Markov-additive chains in R-d*, Statist. Probab. Lett., 47 (2000), pp. 365–380.

[25] J. L. Jensen, *Saddlepoint Approximations*, Oxford Statist. Sci. Ser. 16, Oxford University Press, New York, 1995.

[26] S. Juneja and P. Shahabuddin, *Rare-event simulation techniques: An introduction and recent advances*, Handbooks Oper. Res. Manag. Sci., 13 (2006), pp. 291–350.

[27] A.-K. Kassam and L. N. Trefethen, *Fourth-order time-stepping for stiff PDEs*, SIAM J. Sci. Comput., 26 (2005), pp. 1214–1233, https://doi.org/10.1137/S1064827502410633.

[28] B. Kibler, J. Fatome, C. Finot, G. Millot, F. Dias, G. Genty, N. Akhmediev, and J. M. Dudley, *The Peregrine soliton in nonlinear fibre optics*, Nature Phys., 6 (2010), pp. 790–795.

[29] J. Kuelbs, *Large deviation probabilities and dominating points for open convex sets: nonlogarithmic behavior*, Ann. Probab., 28 (2000), pp. 1259–1279.

[30] F. Lankaš, J. Šponer, P. Hobza, and J. Langowski, *Sequence-dependent elastic properties of DNA*, J. Mol. Biol., 299 (2000), pp. 695–709.

[31] P. Ney, *Dominating points and the asymptotics of large deviations for random walk on* $\mathbb{R}^d$, Ann. Probab., 11 (1983), pp. 158–167.

[32] M. Onorato, S. Residori, U. Bortolozzo, A. Montina, and F. Arecchi, *Rogue waves and their generating mechanisms in different physical contexts*, Phys. Rep., 528 (2013), pp. 47–89, https://doi.org/10.1016/j.physrep.2013.03.001.

[33] A. Picozzi, J. Garnier, T. Hansson, P. Suret, S. Randoux, G. Millot, and D. N. Christodoulides, *Optical wave turbulence: Towards a unified nonequilibrium thermodynamic formulation of statistical nonlinear optics*, Phys. Rep., 542 (2014), pp. 1–132.

[34] L. P. Pitaevsky, *Vortex lines in an imperfect Bose gas*, Soviet Phys. J. Exp. Theoret. Phys., 13 (1961).

Downloaded 09/25/19 to 130.192.92.55. Redistribution subject to SIAM license or copyright; see http://www.siam.org/journals/ojsa.php

Copyright © by SIAM and ASA. Unauthorized reproduction of this article is prohibited.

[35] R.-E. Plessix, *A review of the adjoint-state method for computing the gradient of a functional with geophysical applications*, Geophys. J. Int., 167 (2006), pp. 495–503.

[36] F. Ragone, J. Wouters, and F. Bouchet, *Computation of extreme heat waves in climate models using a large deviation algorithm*, Proc. Natl. Acad. Sci. USA, 115 (2018), 201712645.

[37] S. Randoux, P. Walczak, M. Onorato, and P. Suret, *Intermittency in integrable turbulence*, Phys. Rev. Lett., 113 (2014), 113902.

[38] P. Suret, R. El Koussaifi, A. Tikan, C. Evain, S. Randoux, C. Szwaj, and S. Bielawski, *Single-shot observation of optical rogue waves in integrable turbulence using time microscopy*, Nat. Commun., 7 (2016).

[39] J. Tailleur and J. Kurchan, *Probing rare physical trajectories with Lyapunov weighted dynamics*, Nat. Phys., 3 (2007), p. 203.

[40] A. Tikan, C. Billet, G. El, A. Tovbis, M. Bertola, T. Sylvestre, F. Gustave, S. Randoux, G. Genty, P. Suret, and J. M. Dudley, *Universality of the Peregrine soliton in the focusing dynamics of the cubic nonlinear Schrödinger equation*, Phys. Rev. Lett., 119 (2017), 033901.

[41] F. Tröltzsch, *Optimal Control of Partial Differential Equations*, Grad. Stud. Math. 112, AMS, Providence, RI, 2010.

[42] E. Vanden-Eijnden and J. Weare, *Rare Event Simulation of Small Noise Diffusions*, Comm. Pure Appl. Math., 65 (2012), pp. 1770–1803.

[43] S. R. S. Varadhan, *Large deviations*, Courant Lect. Notes Math. 27, AMS, 2016.

[44] A. Walther, *Automatic differentiation of explicit Runge-Kutta methods for optimal control*, Comput. Optim. Appl., 36 (2007), pp. 83–108.

[45] L. C. Wilcox, G. Stadler, T. Bui-Thanh, and O. Ghattas, *Discretely exact derivatives for hyperbolic PDE-constrained optimization problems discretized by the discontinuous Galerkin method*, J. Sci. Comput., 63 (2015), pp. 138–162.

[46] S. Wright and J. Nocedal, *Numerical Optimization*, Springer Ser. Oper. Res., Springer, Berlin, 2000.

[47] V. E. Zakharov, *Stability of periodic waves of finite amplitude on the surface of a deep fluid*, J. Appl. Mech. Tech. Phys., 9 (1968), pp. 190–194.

[48] V. E. Zakharov, *Turbulence in integrable systems*, Stud. Appl. Math., 122 (2009), pp. 219–234.

Downloaded 09/25/19 to 130.192.92.55. Redistribution subject to SIAM license or copyright; see http://www.siam.org/journals/ojsa.php

Copyright © by SIAM and ASA. Unauthorized reproduction of this article is prohibited.